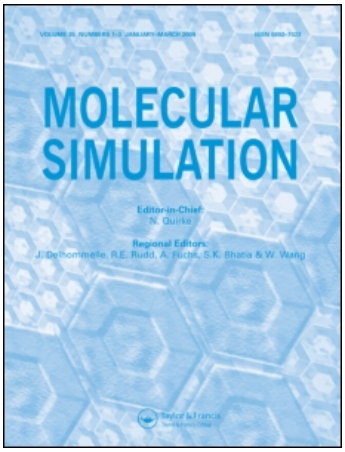

Molecular Simulation
Publication details, including instructions for authors and subscription information:
http://www.informaworld.com/smpp/title~content=t713644482

Recent developments in the molecular modeling of diffusion in nanoporous materials

D. Dubbeldam[a]; R. Q. Snurr[a]
[a] Chemical and Biological Engineering Department, Northwestern University, Evanston, IL, USA

To cite this Article Dubbeldam, D. and Snurr, R. Q.(2007) 'Recent developments in the molecular modeling of diffusion in nanoporous materials', Molecular Simulation, 33: 4, 305 — 325
To link to this Article: DOI: 10.1080/08927020601156418
URL: http://dx.doi.org/10.1080/08927020601156418

Molecular Simulation, Vol. 33, Nos. 4–5, 15–30 April 2007, 305–325

Recent developments in the molecular modeling of diffusion in nanoporous materials

D. DUBBELDAM and R. Q. SNURR*

Chemical and Biological Engineering Department, Northwestern University, 2145 Sheridan Road, Evanston, IL 60208, USA

(Received June 2006; in final form November 2006)

Molecular modeling has become a useful and widely used tool to predict diffusion coefficients of molecules adsorbed in the pores of zeolites and other nanoporous materials. These simulations also provide detailed, molecular-level information about sorbate structure, dynamics, and diffusion mechanisms. We review recent advances in this field, including prediction of various transport coefficients (Fickian, Onsager, Maxwell–Stefan) for single-component and multicomponent systems from equilibrium and non-equilibrium molecular dynamics (MD) simulations, elucidation of anomalous diffusion effects induced by the confining pore structure, and prediction of slow diffusion processes beyond the reach of MD simulations.

Keywords: Molecular modeling; Nanoporous materials; Diffusion; Zeolites; Metal-organic frameworks

1. Introduction

Nanoporous materials are widely used as heterogeneous catalysts and in adsorption and membrane separations [1–4]. Examples include zeolites and other molecular sieves, activated carbons, and clays. Recently, there has been tremendous activity to synthesize new nanoporous materials [5,6]. In particular, one would like to design and synthesize materials having desired functional properties [7]. A particularly interesting strategy that may ultimately allow materials design is to use mild synthesis conditions and well-defined, rigid building blocks that retain their integrity in the final material. These building blocks can be chosen so that they self-assemble into interesting porous structures, ranging from discrete molecular triangles, squares, and cages to extended amorphous or crystalline materials [8–16].

In many applications of nanoporous materials, the rate of molecular transport inside the pores plays a key role in the overall process. A membrane or adsorption separation process exploits differences in rates of diffusion and/or adsorbed-phase concentrations to differentiate between the different molecular species and separate them. For catalytic processes in porous materials, the role of diffusion is well known through the familiar Thiele analysis [17]. For microporous materials (pores less than 20 Å), a number of unusual diffusion effects are observed that have no counter-part in bulk phases. Anisotropic diffusion, the "window" effect, "single-file" diffusion, and other interesting effects arise because of the close interaction between adsorbed molecules and the pore walls. Because of this tight fit, diffusion properties of guest molecules in microporous materials can be quite sensitive to small differences between different host materials, and molecular-level modeling has, therefore, come to be a useful tool for gaining a better understanding of diffusion in nanoporous materials. In this paper, we review recent advances in atomistic modeling of diffusion in nanoporous materials, focusing on two classes of crystalline materials: zeolites and metal-organic frameworks.

Zeolites are crystalline, microporous solids containing cavities and channels of molecular dimensions, typically 3–10 Å in diameter [3]. They have framework structures that are formally constructed from TO_4 tetrahedra that share vertices, where T is a tetrahedrally-coordinated silicon or aluminum atom. Zeolites are widely used in commercial separations, ion exchange, and catalysis applications. Metal-organic frameworks (MOF), sometimes referred to as coordination polymers, are a new class of nanoporous materials synthesized in a building-block approach from metal or metal-oxide vertices interconnected by organic linkers [10,12–15]. The organic linker molecules are typically rigid and contain two or three

*Corresponding author. Email: snurr@northwestern.edu

Molecular Simulation
ISSN 0892-7022 print/ISSN 1029-0435 online © 2007 Taylor & Francis
http://www.tandf.co.uk/journals
DOI: 10.1080/08927020601156418

Table 1. The abbreviations used in this review.

List of abbreviations	
Dc	Dynamically corrected
DCV	Dual control volume
EMD	Equilibrium molecular dynamics
FK-model	Frenkel–Kontorowa model
FT IR	Fourier transform infrared
GCMC	Grand-canonical Monte Carlo
GCMD	grand-canonical molecular dynamics
IAST	Ideal adsorbed solution theory
kMC	Kinetic Monte Carlo
MC	Monte Carlo
MD	Molecular dynamics
MOF	Metal-organic framework
MPC	Molecular path control
MSD	Mean-squared displacement
MTC	Molecular traffic control
NEMD	non-equilibrium molecular dynamics
PFG NMR	Pulsed field gradient nuclear magnetic resonance
QENS	Quasi elastic neutron scattering
TST	Transition state theory

functional groups symmetrically arranged at the ends of the molecules. Because of the extensive literature and know-how from organic chemistry, an incredible variety of candidate linkers exists or can be made. MOF synthesis exploits the directional nature of metal–ligand interactions to provide the desired angle between the linkers. Recent synthetic advances have produced microporous and mesoporous MOFs that are stable when the solvent molecules used in their synthesis are removed from the pores [10,12–15]. This opens up exciting possibilities for applications of MOFs in separations, catalysis, and energy storage [18,19].

Several extensive reviews exist for molecular simulation of diffusion in zeolites [2,20–25], and we, therefore, focus here on some examples of recent developments. Molecular simulation of diffusion in MOFs is still in its early stages, and no reviews exist to date. For convenience we have listed the used abbreviations and nanoporous materials in tables 1 and 2, respectively. This review is organized as follows. Sections 2, 3, and 4 cover the molecular models commonly used, the theoretical frameworks for diffusion in nanoporous materials, and the computation of transport properties by molecular dynamics (MD) simulation, respectively. We then present reviews of MD simulations to calculate diffusion coefficients for mass transport under non-equilibrium conditions, MD simulations to better understand anomalous diffusion, and some development in methods to compute very slow diffusion when MD methods are not applicable. This is followed by a short discussion comparing simulation results with experiment and then conclusions and areas for future development.

2. Molecular models

Most molecular simulations of diffusion in zeolites and MOFs use the popular Kiselev-type potentials [26,27]. In a Kiselev-type model, the host atoms are held rigid at the positions determined by crystallography. Interactions between sorbate molecules and the host are modeled by placing Lennard-Jones sites and partial charges on all atoms of the framework and the sorbate molecules. Often the Lennard-Jones interactions of zeolite Si atoms are

Table 2. Zeolites are designated by three capital letter codes derived from the names of the type materials. For example, MFI denotes the *topology* of the framework. The name is derived from ZSM-5 (Five), a zeolite synthesized by Mobil. The ZSM-5 zeolite contains aluminum and associated nonframework cations, while silicalite is the siliceous form. Both have the MFI topology. The channels in the system are described by specifying the number of tetrahedral silicon (or aluminum) atoms defining the openings. The names of MOFs are often enumerations, e.g. MOF-5, or the metal and the linker are explicitely specified, e.g. Cu-BTC. To date, there is no systematic naming of MOFs.

List of nanoporous materials

Code	*Origin*	*System*	*a,b,c cell lengths (Å)*			*α,β,γ cell angles (°)*		
AFI	Aluminophosphate-Five	1-d (12 T-ring)	13.827	13.827	8.580	90	90	120
BEC	Zeolite Beta-C	3-d (12 T-ring)	12.769	12.769	12.977	90	90	90
BOG	Boggsite	2-d (10,12 T-ring)	20.014	23.580	12.669	90	90	90
CHA	Chabazite	3-d (8 T-ring)	13.675	13.675	14.767	90	90	120
Cu-BTC	Copper (II) benzene-1,3,5-tricarboxylate	3-d MOF	26.343	26.343	26.343	90	90	90
ERI	Erionite	3-d (8 T-ring)	13.054	13.054	15.175	90	90	120
FAU	Faujasite	3-d (12 T-ring)	24.345	24.345	24.345	90	90	90
ITQ-7	Instituto de Tecnologia Quimica Valencia	3-d (12 T-ring)	12.874	12.874	25.674	90	90	120
ISV	ITQ-7 (Seven)	3-d (12 T-ring)	12.874	12.874	25.674	90	90	120
LTA	Linde Type A	3-d (8 T-ring)	11.919	11.919	11.919	90	90	90
LTL	Linde Type L	3-d (8 T-ring)	18.126	18.126	7.567	90	90	120
MFI	ZSM-5 (Five)	3-d (10 T-ring)	20.022	19.899	13.383	90	90	90
MOF-5	Metal-Organic Framework-5	3-d MOF	25.832	25.832	25.832	90	90	90
MTW	ZSM-12 (Twelve)	1-d (12 T-ring)	25.552	5.256	12.117	90	109.312	90
OFF	Offretite	2-d (12,8 T-ring)	13.063	13.063	7.565	90	90	120
SAS	University of Saint Andrews—Six	1-d (8 T-ring)	14.349	14.349	10.398	90	90	90
TON	*T*heta-1 (*On*e)	1-d (10 T-ring)	14.105	17.842	5.256	90	90	90
zeolite T	Intergrowth of ERI and OFF	3-d (12,8 T-ring)						
ZSM-5	Zeolite Socony Mobil—5	3-d (10 T-ring)	20.090	19.738	13.142	90	90	90
ZSM-12	Zeolite Socony Mobil—12	1-d (12 T-ring)	25.552	5.256	12.117	90	109.312	90
Y	FAU with <77 Al per unitcell	3-d (12 T-ring)	24.345	24.345	24.345	90	90	90

neglected, and for non-polar molecules, the Coulomb interactions of all atoms are sometimes neglected. Sorbate–sorbate interaction potentials are often taken from force fields developed for modeling vapor–liquid equilibrium [28,29]. These include any necessary expressions for describing bond-stretching, bond-bending and torsional potentials, as well as Lennard-Jones and partial charge parameters for the atoms of the sorbate molecules. Some researchers have also investigated the effects of allowing the framework atoms to move, with an appropriate potential model for the framework atoms [30–33]. A short overview is given in the introduction of Ref. [34].

The Kiselev-type models are also widely used to predict adsorption isotherms, heats of adsorption and other thermodynamic properties via grand canonical Monte Carlo (GCMC) simulations [27,35]. A common strategy for simulating diffusion in zeolites is to start with a model that reproduces the adsorption isotherms and heats of adsorption. The Kiselev model is attractive because of its simplicity and computational efficiency. Although some researchers have developed more sophisticated models [27], most simulations of diffusion in nanoporous materials today continue to use the Kiselev-type models. Efforts to improve the models have largely focused on optimizing the parameters, especially the sorbate–sorbent Lennard-Jones parameters. An example is shown in figure 1 for the prediction of adsorption isotherms of isobutane in silicalite at various temperatures. The potential parameters and references for experimental data are given in Ref. [36,37]. Reliable force fields optimized for aluminosilicates including sodium, calcium, and proton ions have recently appeared, showing promising quantitative predictions of adsorption properties [38–40]. It has also been reported that models that reproduce single-component isotherms can yield quantitatively correct predictions for mixture adsorption as well [41,42].

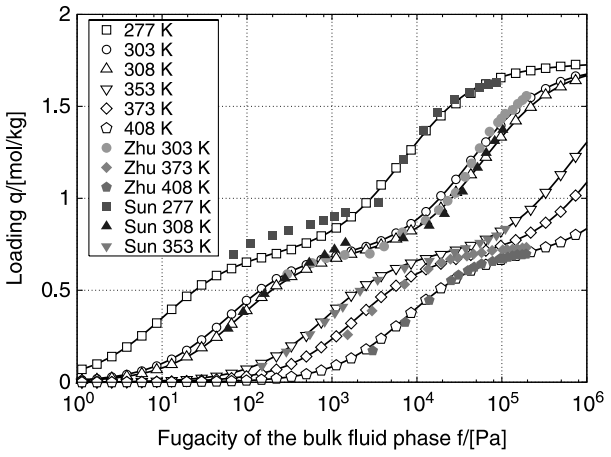

Figure 1. Isotherms of isobutane in silicalite computed with the Kiselev potential model compared to experimental data. Potential parameters and references for experimental data are given in Ref. [36,37]. Reprinted figure with permission from D. Dubbeldam, S. Calero, T. J. H. Vlugt, R. Krishna, T. L. M. Maesen, E. Beerdsen and B. Smit, *Physical Review Letters*, 93, 088302, 2004. Copyright (2004) by the American physical society.

3. Theoretical frameworks for describing diffusion in nanoporous materials

Many different diffusion coefficients can be defined for guest molecules in nanoporous materials, but it is useful to put them into two general classes: transport diffusivities and self-diffusivities. Transport diffusivity describes the transport of mass and the decay of density fluctuations in the system, while self-diffusion describes the diffusive motion of a single particle [2,20,43]. The transport diffusivities are measured under *non-equilibrium* conditions in which finite concentration gradients exist. They are determined by macroscopic measurement methods like gravimetric, volumetric, chromatographic, or frequency-response techniques. In other experiments, the self-diffusivity is measured under *equilibrium* conditions by microscopic techniques, such as quasi elastic neutron scattering (QENS) and pulsed field gradient (PFG) NMR. Using the QENS method it is possible to measure self- and transport diffusivities simultaneously [44]. Most of the early MD simulations in nanoporous materials concentrated on computing self-diffusivities [21]. With growing computer power, the emphasis has gradually shifted toward computing transport diffusivities, which are more relevant for technological applications.

From a phenomenological point of view, there are three different approaches to setting up the flux—driving force relationship for transport diffusion in nanoporous materials under non-equilibrium conditions [45,46]. The formulas presented here are taken from recent publications by Krishna and van Baten [47,48].

i) Fick formulation

In the Fick approach the fluxes **N** are taken to be linearly dependent on the gradients of the loadings ∇c_i of all species with the "constants" of proportionality being the Fick diffusivity matrix D^{T},

$$(\mathbf{N}) = -\rho[D^{\mathrm{T}}](\nabla \mathbf{c}) \tag{1}$$

where N_i is the molecular flux of species i in a mixture consisting of n components in units of molecules $\mathrm{m}^{-2}\,\mathrm{s}^{-1}$, ρ is the framework density in number of unit cells per m^3, c_i is the molecule loading of species i in molecules per unit cell, and D^{T} is the matrix of Fick diffusivities in $\mathrm{m}^2\,\mathrm{s}^{-1}$. The matrix is non-diagonal, and the cross-coefficients represent the coupling between species diffusion. The advantage of using D^{T} is that the Fick relations can be incorporated in the equipment design equations. However, the D^{T} show complex dependences on loading and mixture composition.

ii) Onsager formulation

In the Onsager approach the fluxes are postulated as linear functions of the chemical potential gradients ($\nabla\mu_i$), with the proportionality constants being the Onsager coefficients L_{ij}.

$$(\mathbf{N}) = -[L](\nabla\mu) \tag{2}$$

The Onsager matrix $[L]$ is the square matrix of Onsager elements where $L_{ij}k_BT$ are in units of molecules $m^{-2}s^{-1}$. Here, k_B is the Boltzmann constant and T is the temperature. The Onsager reciprocal relations demand that the matrix $[L]$ is symmetric. It is sometimes convenient to define a modified Onsager matrix $[\Delta]$ [49]

$$(\mathbf{N}) = -\frac{\rho}{k_BT}[\mathbf{c}][\Delta](\nabla\mu) \tag{3}$$

where $[\mathbf{c}]$ denotes the diagonal matrix having c_i as elements. The chemical potential gradients in equation (2) are the true driving force behind diffusive mass transport but may be expressed in terms of the occupancy gradients by introducing a matrix of thermodynamic factors Γ

$$\frac{c_i}{k_BT}\nabla\mu_i \equiv \sum\nolimits_j \Gamma_{ij}\nabla c_j \tag{4}$$

$$\Gamma_{ij} = \frac{c_i}{c_j}\frac{\partial \ln f_i}{\partial \ln c_j} \tag{5}$$

where f_i denotes the fugacity of component i in the bulk fluid phase. The thermodynamic factor can be obtained from the sorption isotherms after differentiation.

iii) Maxwell–Stefan formulation

The Maxwell–Stefan formulation balances diffusive and drag forces, while Fick and Onsager postulate phenomenological flux expressions. Using the Maxwell–Stefan theory, the following expression can be derived for diffusion of species i in a nanoporous material:

$$-\rho\frac{\theta_i}{k_BT}\nabla\mu_i = \sum_{\substack{j=1\\ j\neq i}}^{n}\frac{c_jN_i - c_iN_j}{c_{i,\mathrm{sat}}c_{j,\mathrm{sat}}D_{ij}^{\mathrm{MS}}} + \frac{N_i}{c_{i,\mathrm{sat}}D_i^{\mathrm{MS}}} \tag{6}$$

where $\theta_i \equiv c_i/c_{i,\mathrm{sat}}$ is the dimensionless fractional occupancy of component i, $\nabla\mu_i$ is the force acting on species i tending to move it within the framework, D_i^{MS} is the Maxwell–Stefan diffusivity describing the interaction between component i and the confinement, and D_{ij}^{MS} are the binary exchange Maxwell–Stefan diffusivities describing the correlation effects between components i and j within the framework structure. The correlations are loading and topology dependent. Lower values imply a stronger correlation effect, and for $D_{ij}^{\mathrm{MS}} \to \infty$ correlation effects vanish. For a single component system, D_i^{MS} is sometimes called the "corrected" diffusivity D^C [2]. The Maxwell–Stefan diffusivities can be recast into the Fickian formulation by

$$(N) = -\rho[B]^{-1}[\Gamma](\nabla\mathbf{c}) \tag{7}$$

where the elements of the matrix $[B]$ are

$$B_{ii} = \frac{1}{D_i^{\mathrm{MS}}} + \sum_{\substack{j=1\\ j\neq i}}^{n}\frac{\theta_j}{D_{ij}^{\mathrm{MS}}} \tag{8}$$

$$B_{ij} = -\frac{c_{i,\mathrm{sat}}}{c_{j,\mathrm{sat}}}\frac{\theta_i}{D_{ij}^{\mathrm{MS}}} \quad (i \neq j) \tag{9}$$

and we note that

$$[\Delta] = [B]^{-1} \tag{10}$$

Using the Maxwell–Stefan formulation, a simple expression can be obtained for the self-diffusion D_i^S of species i in a mixture [50,51]

$$D_i^S = \frac{1}{1/D_i^{\mathrm{MS}} + \sum_{j=1}^{n}\theta_j/D_{ij}^{\mathrm{MS}}} \tag{11}$$

This equation can also be viewed as a definition of D_{ii}^{MS}.

The three formulations are strictly equivalent, and all three viewpoints are needed for different purposes. The Fickian formulation is convenient for engineering calculations because the flux equations are written in terms of concentration. The Onsager approach has a strong basis in statistical mechanics, and the Onsager coefficients can be calculated from MD simulations, as described below. One of the chief advantages of the Maxwell–Stefan formulation is that it provides a useful framework for models to predict mixture diffusion based on information from the pure components, especially from D_{ii}^{MS}.

The self-, corrected, and transport diffusivities are equal only in the limit of zero loading. In general one finds that [43]

$$D^{\mathrm{T}} = D^{\mathrm{C}} = D^{\mathrm{S}} \quad \text{for} \quad c = 0 \tag{12}$$

$$D^{\mathrm{T}} \neq D^{C} > D^{S} \quad \text{for} \quad c > 0 \tag{13}$$

The self-diffusivities are more strongly influenced by correlation effects (kinetic and vacancy correlations) than the transport and Maxwell–Stefan diffusivities. In chemical engineering applications it is sometimes assumed that the corrected diffusion coefficient of particles under confinement is independent of loading [2,44,22]. The assumption that the corrected diffusivity is loading-independent is often used to compare different data sets and relate diffusivities measured by microscopic and macroscopic techniques. For a more detailed discussion, see Ref. [52].

4. Calculating diffusion coefficients from molecular dynamics simulations

In MD simulations [53–55], successive configurations of the system are generated by integrating Newton's laws of motion, which then yields a trajectory that describes the positions, velocities and accelerations of the particles as they vary with time. The self-diffusivity describes the motion of an individual particle. In an equilibrium molecular dynamics (EMD) simulation the self-diffusion coefficient D_α^S of component α is computed by taking the slope of the mean-squared displacement (MSD) at long

times

$$D_\alpha^S = \frac{1}{2dN_\alpha} \lim_{t\to\infty} \frac{\mathrm{d}}{\mathrm{d}t} \left\langle \sum_{i=1}^{N_\alpha} (r_i^\alpha(t) - r_i^\alpha(0))^2 \right\rangle \tag{14}$$

where N_α is the number of molecules of component α, d is the spatial dimension of the system, t is the time, and r_i^α is the center-of-mass of molecule i of component α. Equivalently, D_α^S is given by the time integral of the velocity autocorrelation function

$$D_\alpha^S = \frac{1}{dN_\alpha} \int_0^\infty \left\langle \sum_{i=1}^{N_\alpha} v_i^\alpha(t) v_i^\alpha(0) \right\rangle \mathrm{d}t \tag{15}$$

where v_i^α is the center-of-mass-velocity of molecule i of component α. Equation (14) is known as the Einstein equation and equation (15) is often referred to as the Green–Kubo relation. A separation of time scales occurs for interacting particles. At very short time scales the MSD has a quadratic dependence on time (a slope of two on a log–log plot). This is known as the ballistic regime, where particles on average do not yet collide. In nanoporous materials, an intermediate regime starts when particles are colliding, but only with a subset of the other particles. This is due to the confinement. Only when particles are able to escape the local environment and explore the full periodic lattice is the diffusional regime reached. In the diffusive regime, the MSD bends over to attain a different slope and becomes linear with time (a slope of unity on a log–log plot). It is the long-time diffusion coefficient that is of general interest here.

For a single adsorbed component, the transport diffusion coefficient D^{T} is given by

$$D^{\mathrm{T}} = \frac{\Gamma}{2dN} \lim_{t\to\infty} \frac{\mathrm{d}}{\mathrm{d}t} \left\langle \left(\sum_{i=1}^{N} (r_i(t) - r_i(0)) \right)^2 \right\rangle \tag{16}$$

or

$$D^{\mathrm{T}} = \frac{\Gamma}{\mathrm{d}N} \int_0^\infty \left\langle \left(\sum_{i=1}^{N} v_i(t) \right) \left(\sum_{i=1}^{N} v_i(0) \right) \right\rangle \mathrm{d}t \tag{17}$$

The thermodynamic factor Γ is

$$\Gamma = \left(\frac{\partial \ln f}{\partial \ln c} \right)_T \tag{18}$$

and can be obtained from the adsorption isotherm. Isotherms can be obtained experimentally or predicted from GCMC simulations. Alternatively, Γ can be computed during a GCMC simulation as [56]

$$\Gamma = \frac{\langle N \rangle}{\langle N^2 \rangle - \langle N \rangle^2} \tag{19}$$

The omission of the thermodynamic factor in equations (16) and (17), leads to the corrected diffusivity D^c

$$D^C = \frac{1}{2dN} \lim_{t\to\infty} \frac{\mathrm{d}}{\mathrm{d}t} \left\langle \left(\sum_{i=1}^{N} (r_i(t) - r_i(0)) \right)^2 \right\rangle \tag{20}$$

and

$$D^C = \frac{1}{dN} \int_0^\infty \left\langle \left(\sum_{i=1}^{N} v_i(t) \right) \left(\sum_{i=1}^{N} v_i(0) \right) \right\rangle \mathrm{d}t \tag{21}$$

For mixtures, the Onsager Δ elements for components α and β can be computed from equilibrium MD simulations using the Einstein form

$$\Delta_{\alpha\beta} = \frac{1}{2dN_\alpha} \lim_{t\to\infty} \frac{\mathrm{d}}{\mathrm{d}t} \times \left\langle \left(\sum_{i=1}^{N_\alpha} \left(\mathbf{r}_i^\alpha(t) - \mathbf{r}_i^\alpha(0) \right) \right) \left(\sum_{i=1}^{N_\beta} \left(\mathbf{r}_i^\beta(t) - \mathbf{r}_i^\beta(0) \right) \right) \right\rangle \tag{22}$$

or

$$\Delta_{\alpha\beta} = \frac{1}{dN_\alpha} \int_0^\infty \left\langle \left(\sum_{i=1}^{N_\alpha} v_i^\alpha(t) \right) \left(\sum_{i=1}^{N_\beta} v_i^\beta(0) \right) \right\rangle \mathrm{d}t \tag{23}$$

$$= \frac{1}{dN_\alpha} \int_0^\infty \left\langle \sum_{i=1}^{N_\alpha} \sum_{j=1}^{N_\beta} v_i^\alpha(t) v_j^\beta(0) \right\rangle \mathrm{d}t \tag{24}$$

Using equation (10), the elements of $[B] = [\Delta]^{-1}$ can be obtained by matrix inversion. The Maxwell–Stefan diffusivities D_i^{MS} and D_{ij}^{MS} for an n-component system are then given by [48]

$$D_i^{\mathrm{MS}} = \frac{1}{B_{ii} - \sum_{\substack{j=1 \\ j\neq i}}^{n} \theta_j / D_{ij}^{\mathrm{MS}}} \tag{25}$$

$$D_{ij}^{\mathrm{MS}} = -\frac{c_{i,\mathrm{sat}}}{c_{j,\mathrm{sat}}} \frac{\theta_i}{B_{ij}} \tag{26}$$

Equations relating $L_{\alpha\beta}$ (and thus $\Delta_{\alpha\beta}$) to the Fickian diffusion coefficients can also be derived [20].

The Einstein and Green–Kubo equations given above can be applied to each x,y,z-direction individually (when the dimension of the system is taken in each case as $d = 1$), applied to the two dimensional case $d = 2$, or applied to the three dimensional system $d = 3$. In this case the directionally averaged diffusion coefficient is given by

$$D = \frac{D_x + D_y + D_z}{3} \tag{27}$$

Center-of-mass motion for single components can be due to an external field, e.g. the confinement, or due to a lack of linear momentum conservation, e.g. individual components in a mixture. Some thermo- and baro-stat methods are known to violate energy conservation for single components and also momentum conservation in mixtures, causing center-of-mass drift. It is standard practice to remove the

center-of-mass motion from the system at the beginning of an EMD simulation. However, the system may still show center-of-mass drift, and it is desirable to compute the self-diffusivity relative to the center-of-mass motion. To achieve this, self-diffusivities can be computed by

$$D_\alpha^S = \frac{1}{2dN_\alpha} \lim_{t\to\infty} \frac{\mathrm{d}}{\mathrm{d}t} \left\langle \sum_{i=1}^{N_\alpha} \left(\Delta r_i^\alpha(t) - \Delta r_i^\alpha(0)\right)^2 \right\rangle \quad (28)$$

and

$$D_\alpha^S = \frac{1}{dN_\alpha} \int_0^\infty \left\langle \sum_{i=1}^{N_\alpha} \Delta v_i^\alpha(t) \Delta v_i^\alpha(0) \right\rangle \mathrm{d}t \quad (29)$$

where

$$\Delta r_i^\alpha(t) = r_i^\alpha(t) - r^{\mathrm{com}}(t) \quad (30)$$

$$\Delta v_i^\alpha(t) = v_i^\alpha(t) - v^{\mathrm{com}}(t) \quad (31)$$

Here, r^{com} and v^{com} are the displacement and velocity of the center-of-mass of the system, respectively, including the displacement and velocity of the framework itself if the framework atoms are allowed to move. In this case, the drift of the framework should also be subtracted for the corrected and transport diffusivities, equations (16)–(24). Note that for diffusion in disconnected channel systems that are unable to exchange momentum, the equations apply individually, i.e. the center-of-mass drift is to be computed per channel system.

In simple fluids there is only a time scale separation for the self-motion, not for the transport motion. In nanoporous materials, both the displacements of the single particles as well as the displacements of the total center of mass are restricted by the confinement, and a time scale separation is also present in transport diffusion. This is very much related to the diffusion of polymers in melts where similar time scale separations occur [57]. The time scale separation is shown in figure 2 for the self- and corrected diffusion of benzene in MOF-5 at room temperature. MOF-5 contains two alternating cavities of about $\lambda_1 = 10.9$ Å and $\lambda_2 = 14.3$ Å in diameter (figure 3). The structure is cubic, and diffusion in MOF-5 is isotropic ($D_x = D_y = D_z$). As a rule of thumb, the diffusional regime (i.e. a slope of unity on a log–log plot) is obtained after the mean-square displacement has reached at least λ^2, where λ is the length of the largest repeating cavity. For cage-like nanoporous materials the MSD thus obtained can be fitted taking the time corresponding to λ^2 as the minimum. Note that accuracy in the calculated MSD decreases as time t is increased. The time where the diffusional regime starts can be as high as several nanoseconds in carbon nanotubes [58,59], even though diffusion is orders of magnitude faster than in zeolites [60–62]. It is also possible to estimate a starting point for calculating diffusive behavior more systematically [63].

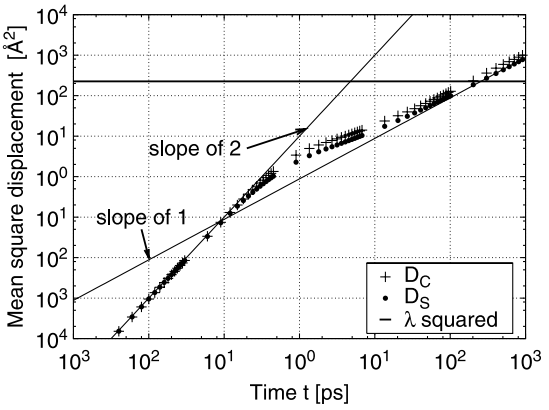

Figure 2. MSD for the self-diffusivity D^S and the corrected diffusivity D^C for benzene in MOF-5 at 298 K at an average loading of 4 molecules per cavity. MOF-5 contains two alternating cavities of about $\lambda_1 = 10.9$ Å and $\lambda_2 = 14.3$ Å in diameter. For reference, we also show λ^2, with $\lambda = 14.3$ Å. The dotted lines are of slope two (the "ballistic" regime), and of slope unity (the "diffusive" regime), respectively. The potential parameters are similar to Ref. [98].

5. Review: transport diffusion of single components and mixtures

Early simulations of diffusion in zeolites focused on calculation of the self-diffusivity for single adsorbed components using EMD simulations [21]. The field progressed from simple spherical molecules to more complicated adsorbates and from all-silica zeolites to more complicated cation-containing materials. MD simulations of

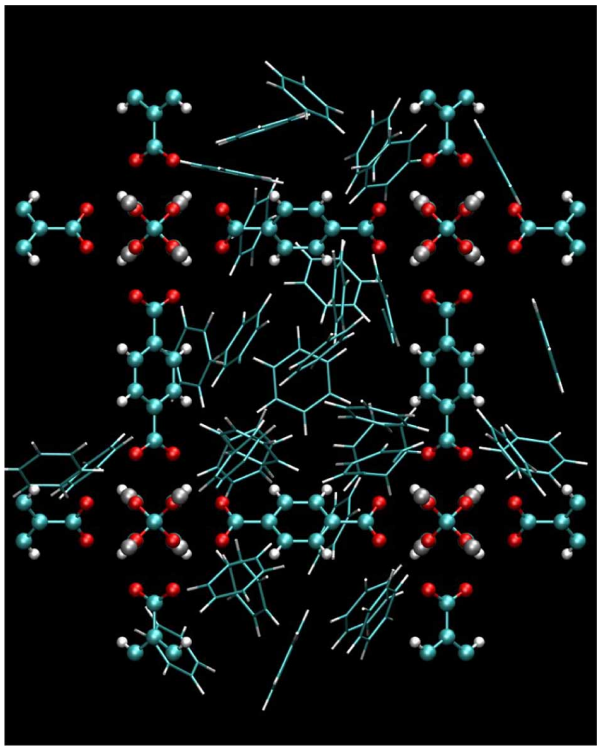

Figure 3. Typical snapshot of benzene molecules in MOF-5 at a loading of four molecules per cavity at room temperature. For clarity the linker molecules (the BDC molecules) and the corner clusters are shown disconnected; both are rendered as stick-and-balls. The corner clusters contain four zinc atoms surrounding a central oxygen atom and form the vertices of the framework.

the self-diffusion of mixtures in zeolites have also been reported [64–66].

The first attempts to compute Fickian diffusivities in zeolites were reported by Maginn *et al.* in 1993 for methane in silicalite [67]. Equations (20) and (21) were already in use in other fields [68], but Maginn *et al.* did not find them to be viable for application in zeolites with the computers of the time. Note that self-diffusion can be averaged over all the particles of the systems, whereas the center-of-mass diffusion cannot (a single-particle property vs. a system property). Instead, Maginn *et al.* developed two non-equilibrium MD methods, one involving the relaxation of a concentration gradient in the simulation box and another using an external force applied to the molecules and equivalent to a chemical potential gradient. Fritzsche *et al.* applied a concentration gradient in an MD simulation to calculate the transport diffusivities of methane in LTA zeolite [69]. Dual-control-volume grand canonical molecular dynamics simulations (DCV GCMD) [70,71] have also been applied to zeolite systems to calculate the transport diffusivities [72].

With dramatically increasing computer power in recent years, it has become possible to use equations (20) and (21) to calculate transport diffusivities in zeolites from equilibrium MD simulations, and we describe some examples in this section. In a critical comparison, Arya *et al.* found that the overhead involved in the computation of transport properties through the DCV GCMD method made it less efficient than EMD methods or external field non-equilibrium MD (NEMD) methods [73]. Chempath *et al.* recently demonstrated that, the external field NEMD method is more efficient than EMD for mixtures [74].

Tepper and Briels showed that the corrected diffusivities D^C might be interpreted as a sort of center-of-mass diffusion times the number of molecules, but only when periodic boundaries are employed [75]. Moreover, they presented wavevector-dependent versions of the above equations, applied them to the calculation of transport diffusion in a channel-type zeolite AFI, and found a regime where the measured diffusivities were independent of the wave vector k [76]. Another k-dependent treatment was published by Sholl [77]. In the hydrodynamic regime all transport properties are independent of the wavelength, while in the generalized hydrodynamic regime the transport coefficients become k-dependent [78]. The analysis by Tepper *et al.* showed that surprisingly long channels are needed to extract reliable diffusion coefficients in unidimensional systems.

A long-standing question about diffusion in zeolites is the concentration dependence of the corrected diffusivity for single components. As noted above, it is sometimes assumed that the corrected diffusivity is independent of concentration. Several approaches have been taken to answer this question, including the use of QENS, MD simulation, kinetic Monte Carlo (kMC) simulations, and the Reed–Ehrlich model [79]. The Reed–Ehrlich model [56] for surface diffusion is a lattice model accounting for inter-molecular forces, introduced to nanoporous materials by Krishna. In the model, the jump rates of species i are influenced by the presence of neighboring molecules by a factor $f_i = \exp(-\Delta U_i/k_BT)$, where ΔU_i denotes the change of the energy barrier to diffusion resulting from the presence of other adsorbed molecules. The Maxwell–Stefan diffusivity (equivalent to the corrected diffusivity for a single-component system) as a function of the fractional loading can be written as

$$D_i^{\mathrm{MS}}(\theta_i) = D^{\mathrm{MS}}(0)\frac{(1+\epsilon_i)^{z-1}}{(1+\epsilon_i f_i)^z} \tag{32}$$

where ϵ and β are dimensionless Reed–Ehrlich parameters defined as

$$\epsilon_i = \frac{(\beta - 1 + 2\theta_i)}{2(1-\theta_i)f_i} \tag{33}$$

$$\beta = \sqrt{1 - 4\theta_i(1-\theta_i)(1-f_i)} \tag{34}$$

The coordination number z reflects the number of nearest neighbors and needs to be determined carefully. Although the Reed–Ehrlich equations are a model for surface diffusion, the model has been successfully applied to describe diffusion in nanoporous materials [79,46,80].

Through the Maxwell–Stefan Reed–Ehrlich formulation, a direct relation can be made between the adsorption isotherms and diffusion behavior. For example, Krishna *et al.* investigated the inflection, in both the adsorption isotherm and in the corrected diffusivity over loading, of CF_4 in MFI at a loading 12 molecules per unit cell [81]. They studied the underlying reasons by performing kinetic Monte Carlo simulations and showed that at 12 molecules per unit cell the molecular traffic along the zigzag channels comes to a virtual stand-still and further transport occurs only along the straight channels of MFI. See figure 4 for the structure of MFI and the adsorption lattice sites for CH_4 and CF_4.

Understanding multicomponent diffusion in zeolites is important for technological applications. Unfortunately, measurements of the multicomponent diffusivities are difficult, and there is little data available in the literature. MD simulations have, therefore, played an important role in recent years in improving our understanding of multicomponent diffusion in zeolites. For example, Sanborn and Snurr calculated the transport diffusivities and Onsager coefficients of binary mixtures of CF_4 and *n*-alkanes in the zeolite faujasite [82]. They compared equations (22) and (24) and found good agreement between both results. In a succeeding paper, they again studied a CF_4-methane mixture in faujasite, but now at various loadings [83]. They used equation (1) to determine the flux through a membrane of macroscopic dimension and concluded that neglecting the cross-term coefficients (with $i \neq j$) can lead to quantitative and sometimes even qualitative errors.

A major goal for multicomponent systems has been to predict mixture behavior from single-component data. Krishna and coworkers used the Maxwell–Stefan approach to formally disentangle the i–i and i–j

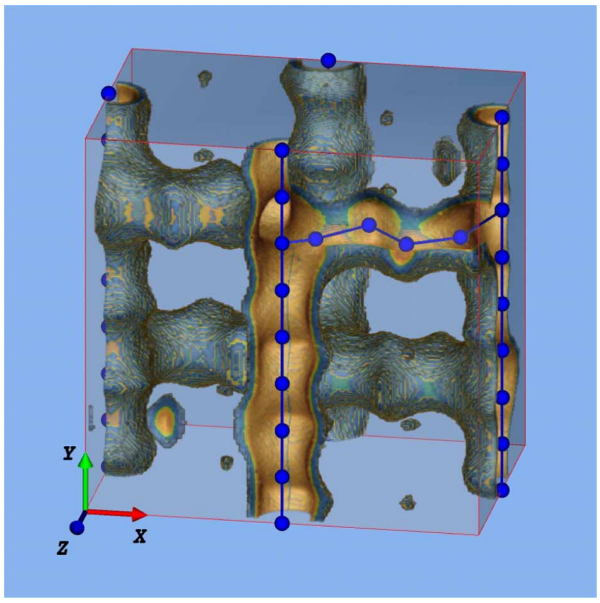

Figure 4. The structure of the MFI-zeolite topology (the siliceous form is known as silicalite, the aluminosilicate form is known as ZSM-5). MFI has linear channels intersected with zig–zag channels four times per periodic unit cell. At low methane loadings, there are four favorable positions per straight channel and four per zigzag channel, making the total number per unit cell 16. At higher loadings the number of preferential methane sites is 32. The lattice for CF_4 is the same, but a CF_4 molecule prevents the neighboring sites from being filled simultaneously because of the higher repulsion of the bulkier CF_4 molecules [97]. The dimensions of the cell are 20.022 × 19.899 × 13.383 Å. Figure courtesy of E. Beerdsen. Reprinted figure with permission from E. Beerdsen, D. Dubbeldam, and B. Smit, *Physical Review Letters*, 95, 164505, 2005. Copyright (2005) by the American physical society.

interactions in a mixture. This allowed them to develop a model for estimating the mixture exchange coefficient D_{ij}^{MS} from the values of the self-exchange coefficients D_{ii}^{MS} and D_{jj}^{MS}. (See Refs. [46,84,85] and references therein.) The model, therefore, allows the possibility of estimating the transport behavior of multicomponent mixtures on the basis of information from single-component data on D_i^C and D_i^S [84]. For example, D_{12}^{MS}, D_{23}^{MS} and D_{13}^{MS} in a ternary mixture are related to the coefficients in the binary mixture, and these are in turn related to the coefficients of the pure components at the total mixture occupancy. Much of the current research effort on mixture diffusion focuses on the interpolating function and its validation with molecular simulations. Skoulidas *et al.* proposed a logarithmic interpolation formula for two component mixtures [84], later extended by Krishna and van Baten for use in *n*-component mixtures [48]

$$c_{j,\mathrm{sat}}D_{ij}^{\mathrm{MS}} = \left[c_{j,\mathrm{sat}}D_{ii}^{\mathrm{MS}}\right]^{c_i/(c_i+c_j)}\left[c_{i,\mathrm{sat}}D_{jj}^{\mathrm{MS}}\right]^{c_j/(c_i+c_j)} \qquad (35)$$

Krishna and co-workers showed that the Maxwell–Stefan diffusivities D_i^{MS} have nearly the same value for species *i* whether this species is present on its own or in a mixture with several species, when evaluated at the *same* fractional loading θ [48,74]. For mixtures, the D_{ii}^{MS} and D_{jj}^{MS} are to be determined from the total occupancy of the mixture. Combination with the ideal adsorbed solution theory (IAST) [86], for estimating multicomponent sorption equilibria from single-component sorption, allows the estimation of the Fick transport diffusivities for multicomponent mixtures. This approach successfully reproduces multi-component diffusivities from only single component diffusivities and multi-component isotherm data for the systems tested to date, using the logarithmic interpolation equation (35) [46–49,74,80,81,84,85,87–91]. Recently, Sholl tested the validity of the logarithmic interpolation function for zeolites having a combination of strongly and weakly adsorbing sites. He computed single-component and binary mixture diffusion coefficients using kinetic Monte Carlo for a two-dimensional lattice model over a wide range of lattice occupancies and compositions. He found the formula to be accurate in situations where the spatial distribution of binding site energies is relatively homogeneous, but considerably less accurate for strongly heterogeneous energy distributions [92].

In the past five years, the calculation of transport diffusivities has moved from cutting edge to almost routine, and several papers have appeared featuring systematic MD studies of transport diffusivities as a function of loading and composition in different nanoporous materials. Skoulidas and Sholl used atomistic simulations to examine the adsorption isotherms, self-diffusivities, and transport diffusivities of seven light gases, CH_4, CF_4, He, Ne, Ar, Xe, and SF_6, adsorbed as single-components in silicalite at room temperature [93]. The main conclusions were that the corrected diffusivities decreased while the transport diffusivities increased with loading. The approximation that the corrected diffusivity is loading independent was found to be generally incorrect. However, they did find that methane in silicalite was well approximated by the loading-independence approximation, in line with the earlier result for the same system by Maginn *et al.* [67]. They also noted that the ability of a lattice-gas model to accurately reproduce the loading dependence of the self-diffusivity does not imply that the same model accurately captures the corrected and transport diffusivities for that adsorbate. Skoulidas and Sholl explored how the zeolite structure and connectivity affect diffusion by computing self-, corrected, and transport diffusivities of CH_4, CF_4, SF_6, Ar, and Ne in silicalite; CH_4, Ar, and Ne in ITQ-3; CH_4, CF_4, Ar, and SF_6 in ITQ-7; and CH_4, CF_4, Ar, and H_2 in ZSM-12 at room temperature [94]. The broad data set presented was useful for considering the variety of diffusion behaviors that can occur for small molecules adsorbed in zeolite pores. The paper raised interesting questions as to how and why the pore structure affects the changes in diffusion with loading.

The data and simulations of Skoulidas and Sholl motivated Beerdsen *et al.* to develop approximate criteria that predict the trends that will arise from such simulations and experiments. Beerdsen *et al.* constructed a classification of pore topologies based on a free energy match between the molecule and the structure of the confinement [95,96]. An example classification was provided for

methane by using MD and dynamically-corrected transition-state theory (dcTST) simulations in 10 different sieve topologies: LTA, CHA, ERI, SAS, AFI, MTW, LTL, MFI, BOG, and BEC. The classification and the rational why diffusion for methane increases, decreases, or stays constant with changing loading will be discussed later.

The work by Beerdsen *et al.* showed another important principle: the self- and corrected diffusivity always sharply drop near maximum loading. This was well accepted for self-diffusion, but as noted, for corrected diffusion the debate was open. However, if self-diffusivity comes to a halt because none of the particles is able to move at such a high loading then so must the corrected diffusivity. Because the corrected diffusivity is related to the center-of-mass motion, it is clear that if no particle is able to move, then the center-of-mass cannot change either, see equation (20). Even for systems where the corrected diffusivity was generally thought to be independent of loading (such as methane in MFI), Beerdsen *et al.* [97] showed that at high enough loadings, both self- and corrected diffusivities sharply decrease (figure 5), and eventually drop to a level comparable to solid diffusion. Based on this, Beerdsen *et al.* defined the maximum loading as the loading where the diffusion (both self and corrected) becomes comparable to solid diffusion. This maximum is generally much higher than an estimate based on an adsorption isotherm at experimentally accessible pressures [97].

The simulations in figure 5 have been run sufficiently long for the error bar to be smaller than twice the symbol size. Therefore, the irregular behavior of the diffusion coefficients is not the result of poor statistics, but an intrinsic phenomenon in these systems. It has some very characteristic features that could easily be dismissed as "noise". Detailed inspection of the components of the diffusion coefficients shows that the humps in the directionally-averaged value can be related to events in one of the components. It is possible to attribute each hump to a reordering of the adsorbed molecules, often being a transition in the number of available adsorption sites. This shows that the number and type of adsorption sites is in general a function of loading. An increase in $D^{C,y}$ is observed, caused by the "freezing" of particles in the zigzag channels that "smoothens" the straight channels and a transition to a different adsorption lattice beyond a loading of 16 molecules per unit cell.

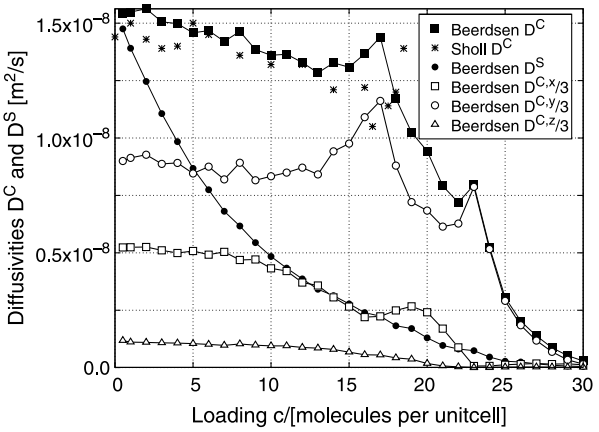

Figure 5. Corrected and self-diffusivities of CH_4 in MFI-type zeolite at 300 K, from MD simulations of Beerdsen *et al.* [97] and Skoulidas and Sholl [93]. An increase in the $D^{C,y}$ is observed, caused by the "freezing" of particles in the zigzag channels. These particles reduce the diffusion in *x*- and *z*-direction, but also "smoothen" the straight channels resulting in an increase in *y*-diffusion. Note that after 16 molecules per unit cell a transition from a lattice of 16 molecules per unit cell to a lattice of 32 molecules per unit cell takes place, as shown in figure 4. Reprinted figure with permission from E. Beerdsen, D. Dubbeldam, and B. Smit, *Physical Review Letters*, 95, 164505, 2005. Copyright (2005) by the American physical society.

The first MD simulations in MOFs were performed by Sarkisov *et al.* [98] and Skoulidas [99]. Sarkisov *et al.* reported self-diffusion coefficients in MOF-5 for methane, *n*-pentane, *n*-hexane, *n*-heptane and cyclohexane. They were found to be of the same order of magnitude as in silicalite. Almost simultaneously, Skoulidas reported diffusion of argon in another MOF, Cu-BTC [99]. This study probed the dependence of self- and transport diffusion over a wide range of pore loadings at room temperature. The two diffusivities differed by almost two orders of magnitude at high pore loadings. Skoulidas and Sholl continued with an extensive report on diffusion of light gases in several MOFs as a function of pore loading [100]. They studied Ar, CH_4, CO_2, N_2, and H_2 diffusion in MOF-2, MOF-3, MOF-5, and Cu-BTC. Their results greatly expanded the range of MOFs for which data describing molecular diffusion is available. Yang and Zhong performed a systematic molecular simulation study on the adsorption and diffusion of hydrogen in MOFs to provide insight into molecular-level details of the underlying mechanisms [101]. Their work shows that metal-oxygen clusters are preferential adsorption sites for hydrogen in MOFs, and the effect of the organic linkers becomes evident with increasing pressure.

Very recently, the first experimental data on diffusion in MOFs became available. Stallmach *et al.* reported a PFG NMR study on diffusion of hydrocarbons in MOF-5 [102]. They demonstrated experimentally that organic gas molecules diffuse quite rapidly in MOFs. Their measurements for *n*-hexane were in good agreement with the simulation results of Sarkisov *et al.* [98], but the results for methane were about an order of magnitude higher. It is interesting to note that MD simulations of diffusion in MOFs appeared almost two years before the first experimental report.

6. Review: anomalous diffusion effects in nanoporous materials

Diffusion of adsorbates inside nanoporous materials can be very different from bulk fluid behavior. In fluids, diffusivities generally decrease with chain-length and molecular weight, and diffusion is isotropic. Several interesting effects have been found in nanoporous materials that are clearly due to the confinement.

We discuss several examples here: single-file diffusion, the window effect and incommensurate diffusion, molecular traffic control (MTC), molecular path control (MPC), and levitation effects.

Single-file diffusion occurs in unidimensional channel systems if molecules are too bulky to pass each other. The MSD becomes proportional to the square-root of the time rather than to time as in normal diffusion [103–105]. Various examples of single-file diffusion can be found: ion transport in biophysics [106], surface diffusion on crystal surfaces [107], diffusion in zeolites [108–110], and colloids in one-dimensional channels [111]. Experimentally, there was some debate whether methane would display single-file diffusion in the channels of the AFI-type zeolite. Kukla *et al.* reported that it did from PFG NMR measurements [108], but this was later contradicted by experiments of Nivarthi *et al.* [112] and Jobic *et al.* [113]. The simulations of Hoogenboom *et al.* [76] indicated these discrepancies could be related to differences in times scales probed by the experiments. Larger molecules than methane are known to show single-file diffusion in AFI-type zeolites [114]. Recently, it has been proposed that single-file diffusion in one-dimensional zeolite channels might find practical application in trapping of small molecules by larger ones for treating automotive exhaust [115].

The *window* effect is one of the most controversial and intriguing phenomena in the zeolite literature. Chen *et al.* discovered in 1968 that ERI-type zeolites yield a bimodal product distribution when cracking long alkanes, with maxima at *n*-C_{3-4} and *n*-C_{10-12} but no products in the C_{5-8} range (the *window*) [116,117]. Conventional zeolite-catalyzed (hydro)cracking yields a product distribution with only a single maximum, which is consistent with the currently accepted reaction mechanisms [118,119]. For a long time the window effect has been attributed almost exclusively to the diffusion rate of *n*-alkanes in ERI-type zeolites. Gorring claimed that the product distribution and the diffusion coefficient as a function of *n*-alkane length correlate extremely well [120]. Surprisingly, the diffusion rates reportedly increase significantly going from C_8 to C_{12} before the usual monotonic decrease with chain length sets in, as shown in figure 6. The low diffusion coefficients for *n*-C_7 to *n*-C_9 suggest that these molecules diffuse too slowly to leave the zeolite without cracking; the high diffusion coefficients for *n*-C_{10} to *n*-C_{12} suggest that these molecules diffuse rapidly enough to escape. According to Gorring the diffusion rate exhibits a maximum for C_{12} because the shape is incommensurate with that of an ERI-type cage, so that C_{12} is always inside an ERI-type window. Smaller molecules are commensurate with the ERI-type cage and remain trapped within a single cage.

Simulations show that the origin of the window effect is a relatively unfavorable adsorption for the chain lengths close to the cage size combined with a low orientational freedom as the chains are stretched across a cage tethered at opposite windows [121,122]. As the movement of the incommensurate chain is less impeded by the higher free energy barriers a commensurate chain would feel, it has an enhanced mobility around integer values of the ratio of the chain length to the period of the lattice. Perhaps the simplest model for molecules that are either commensurate or incommensurate with the framework structure is the 1938 Frenkel–Kontorowa (FK) model [123–126] for adsorbed atoms on a periodic substrate. The model, consisting of a string of atoms connected by springs and subjected to a periodic potential, predicts a "floating phase" with very low energy barriers when the ratio *a*/*b* is non-integer, where *a* is the equilibrium lattice spacing of the harmonic chain and *b* the lattice period. Several models, similar in spirit to the FK model but differing in complexity, have been proposed by Ruckenstein and Lee [127], Derouane *et al.* [128], and Nitsche and Wei [129].

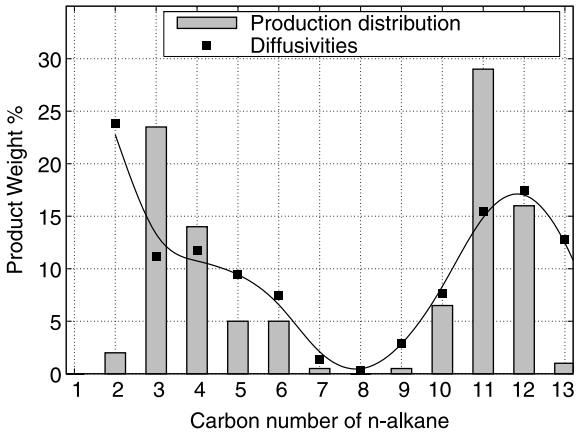

Figure 6. The window effect in ERI-type zeolites: a near-perfect correlation was found between the product distribution seen by Chen *et al.* [116,117] and the diffusion coefficient as a function of *n*-alkane length measured by Gorring [120]. However, Gorring's diffusion measurements were likely effected by non-linearity, extra-crystalline diffusion, and heat effects, and probably should be considered as unreliable [132].

Diffusion measurements by Cavalcante *et al.* [130] and Magalhães *et al.* [131] did not reproduce the increase in diffusion coefficient for the appropriate *n*-alkane lengths, as shown in figure 7. However, the view-point that window-effects do not exist is becoming less common in the literature, and it would be hard to make that case based on two experimental studies that did not corroborate the window-effect in such a complicated system as zeolite T. Zeolite T is an inter growth of offretite and erionite, where erionite are considered as stacking faults within the offretite channel-system and form bottlenecks for diffusion. The studied systems were similar, but not equivalent to Gorring's system. To complicate matters further, Gorring's measurements were likely affected by non-linearity, extra-crystalline diffusion, and heat effects, and probably should be considered as unreliable [132].

It is interesting to observe that there is good agreement between simulation results (figure 7) and the results of Gorring in ERI- and CHA-type zeolites for the chain length of the minima and maxima for diffusion of *n*-alkanes, although the magnitudes of the diffusivities differ [121,133]. These simulations suggest that the crossover points, at which a chain fits in n cages and a longer one into $(n+1)$ cages, are

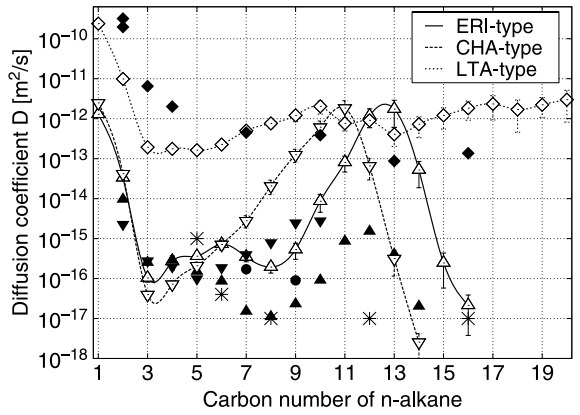

Figure 7. Diffusion coefficients at small loadings as a function of chain length at 600 K for ERI-, CHA-, and LTA-type zeolite; △ ERI-type silica sim. results [121,133], ▲ exp. results of Gorring [120], ∗ Cavalcante *et al.* [130], • Magalhães *et al.* [131]; ▽ CHA-type silica sim. results [121,133], ▼ exp. results of Gorring [117]; ◇ LTA-type silica sim. results [121,133], ◆ exp. compiled in Ref. [2].

directly related to the local minima in the Henry coefficients, the heats of adsorption, and the activation energies, and to the local maxima in the diffusion coefficients and the frequency factors. Recently, the first experimental confirmations of the window effect were found in less complex systems, such as LTL zeolite by Yoo *et al.* [134] and LTA-5A by Jobic *et al.* [135]. Yoo *et al.* detected a periodic dependence of the diffusion coefficient on the number of carbon atoms in the alkane, relating this effective size of the molecule to the size of a single channel period. Jobic *et al.* found experimental evidence of the increase in diffusion in LTA around chain length C_{10-12} as predicted by previous simulation work [121,133]. It is uncertain if this result can be related to the window effect as the match between the effective sorbate length and the cage length is unclear. This is certainly an interesting area for future work.

Other researchers have discussed related effects under the name of (in)commensurate diffusion or "resonant diffusion" [127]. In a recent article by Tsekov and Evstatieva, some theoretical models were reviewed [136]. A general formula for calculation of the diffusion coefficient of a particle moving in the field of a periodic potential was developed, which takes into account both the potential barrier effect and the dependence of the friction coefficient on the potential. The application of the theory to the diffusion of dimers on solid surfaces reveals a nonmonotonic dependence of the diffusion coefficient on the ratio between the dimer and solid spatial parameters. Earlier, Tsekov and Smirniotis theoretically studied diffusion of normal alkanes in one-dimensional zeolites on the basis of the stochastic equation formalism [137]. The calculated diffusion coefficient accounts for the vibrations of the diffusing molecule and zeolite framework, molecule–zeolite interaction, and specific structure of the zeolite. It was shown that when the interaction potential is predominantly determined by the zeolite pore structure, the diffusion coefficient varies periodically with the number of carbon atoms in the alkane molecule. Runnebaum and Maginn conducted a MD study of *n*-alkane dynamics in the zeolite silicalite [138]. Chains ranging in length from *n*-C_4 to *n*-C_{20} were examined at various loadings and temperatures. An interesting chain-length dependence for the individual components of the self-diffusivity tensor was observed. While the self-diffusivities of chains in the *x*- and *z*-directions exhibit a monotonic decrease as a function of chain length, the self-diffusivity along the *y*-axis is a periodic function of chain length. Local maxima in the self-diffusivity along this axis occur for *n*-C_8 and *n*-C_{16}, while local minima are observed for *n*-C_6 and *n*-C_{14}. The apparent activation energy for diffusion is also periodic with chain length. Periodicity in the diffusivity and activation energies are most pronounced at low temperature. A physical explanation for this behavior was given in terms of a resonant diffusion mechanism. Talu *et al.* used the steady-state single-crystal membrane technique to measure the diffusive flux in the *z*-direction through a single-crystal silicate membrane and found excellent agreement [139] with Runnebaum and Maginn. The results were also confirmed by Jobic [140], who measured the diffusivities of long *n*-alkanes in ZSM-5 by QENS. Self-diffusion coefficients and activation energies for chains up to C_{14} were obtained. The agreement with single-crystal membrane experiments was reasonable, except for C_6. The recent work of Krishna *et al.* [81] and Beerdsen *et al.* [97] also shows the increase in *y*-diffusion due to the "smoothening" of the channels as the loading or chain length is changed.

Related to the window effect is the "levitation effect" [141–143]. Sorbates diffusing in zeolitic cavities have been found to show nonmonotonic dependence of the self diffusivity D^S on the Lennard-Jones sorbate size σ. In fact, this dependence exhibits two distinct regimes. For small sorbates, D^S is found to be proportional to $1/\sigma^2$ and thus, decreases with increasing sorbate size. This regime has been termed the linear regime. For larger sorbate sizes, D increases unexpectedly, and then decreases steeply as σ is further increased. This is termed the anomalous regime. Molecular dynamics studies on linear molecules of different lengths l in zeolite NaY at 140 and 200 K have shown that there is a peak in D^S as a function of l, suggesting that the levitation effect exists for linear molecules, in addition to simple spherical molecules [144]. The large cross-term diffusivities in binary mixtures confined to zeolite NaY were also attributed to the levitation effect [145].

The concept of MTC was originally postulated by Derouane and Gabelica[146] to explain why some reactions in nanoporous materials were apparently free of counter-diffusion limitations. They proposed that reactants would enter through one type of pore and products would exit through another type as shown in figure 8. This concept was debated in the literature but never convincingly established. In particular, the early evidence supporting the idea was all indirect, involving static thermodynamic, rather than diffusional properties. The first dynamical support for MTC was provided by Clark *et al.* [147] using MD

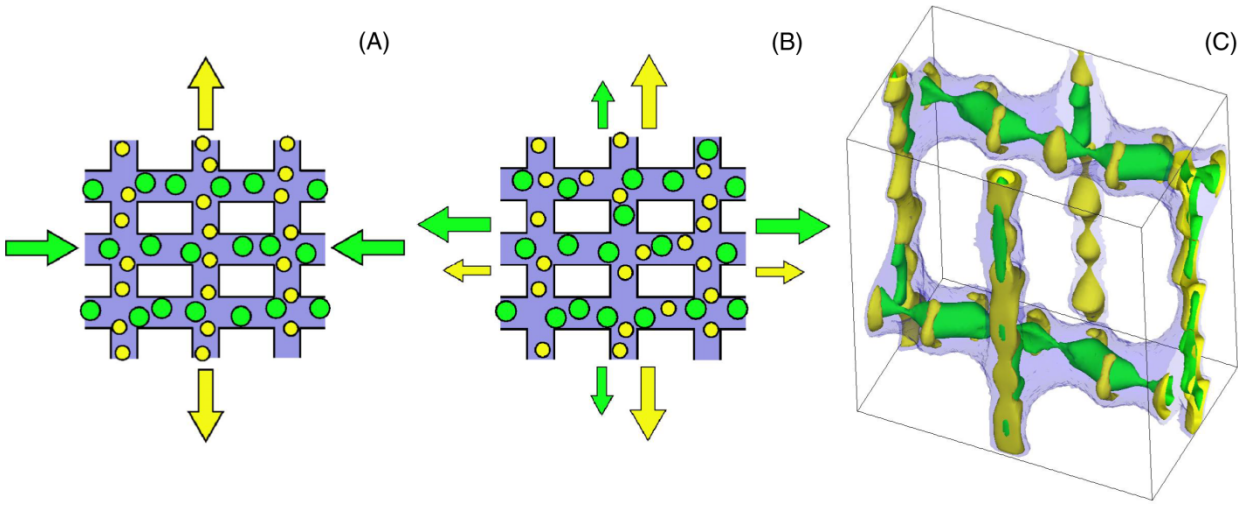

Figure 8. (A) Molecular traffic control (MTC) in nanoporous materials. Green reactant molecules diffuse in through one set of channels, while yellow product molecules diffuse out unhindered. (B) The equilibrium analog, eqMTC. (C) Probability densities from a simulation in the model system (BOG-type zeolite) are shown for SF_6 (green, large molecule), and xenon (yellow, small molecule). Each contour encloses 75% of the most probable center-of-mass position density. Pore shape shown as transparent contour [147]. Figure courtesy of L.A. Clark. Reprinted figure with permission from L. A. Clark, G. T. Ye, and R. Q. Snurr, *Physical Review Letters*, 84, 2893–2896, 2000. Copyright (2000) by the American physical society (colour in online version).

simulations. First, Clark *et al.* used equilibrium MD to investigate what they termed "equilibrium MTC." As a model system, they chose Lennard-Jones particles (xenon and SF_6) in BOG zeolite, which has intersecting channels of different pore diameter. Their equilibrium MD simulations showed that xenon diffuses preferentially in the smaller channels and SF_6 diffuses faster in the larger channels. This is not necessarily the expected result, because one might simply expect xenon to diffuse faster than SF_6 in both channel directions. Clark *et al.* provided a more precise set of criteria to define equilibrium MTC and investigated the molecular-level causes of the effect. They also performed a simple non-equilibrium simulation that more closely mimics the original MTC idea (but without reactions). A large equilibrium MTC system (2085 molecules) was equilibrated using MD and normal periodic boundary conditions. Then the periodic boundary conditions were turned off, and the molecules were allowed to diffuse out into the (initially) empty surrounding zeolite for 1.0 ns. The initial and final configurations are shown in figure 9. It can be seen that this system shows highly anisotropic diffusion consistent with MTC. The large SF_6 molecules diffuse almost exclusively in the wide pore direction (horizontal), while the small xenon molecules diffuse predominantly in the narrow pore direction (vertical). Since reaction is unlikely to change this behavior and anisotropic behavior is perhaps even more likely for molecules of different shape, the result provides support for Derouane's original MTC idea. Recently, some theoretical progress has been made to evaluate the effect of MTC diffusion effects on catalysis in zeolite crystals [148–150].

A related phenomenon that also deals with diffusional anisotropy is MPC. Dubbeldam *et al.* performed MD simulations in erionite-type zeolites [151,152] and found that, depending on loading, molecules follow a preferred pathway. It can, therefore, be viewed as an analogue of MTC for a single component. It reinforces the idea that the confinement a particle feels is due to the framework and due to other particles. They found a reversal of anisotropy, i.e. at low loading the diffusivity in the z-direction is two times faster than in the xy-direction for both the self- and corrected diffusivity, while for higher loadings this changes into a z-diffusivity that is more than two times slower. The conclusion is that the effective pore system changes with loading. The interesting aspect is that this behavior is due to a complete change in the diffusion mechanism, as shown in figure 10, and that the degree of anisotropy can be controlled by a simple change in pressure (loading). MPC is an interesting example of how the loading may dramatically affect the molecular trajectories in nanoporous materials.

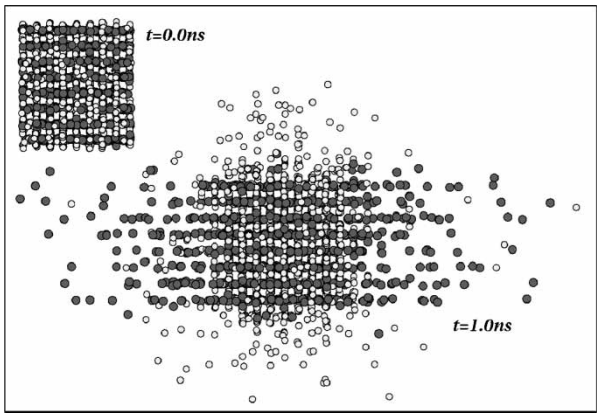

Figure 9. Relaxation of xenon and SF_6 in BOG zeolite from a non-equilibrium MD simulation, supporting the anisotropic diffusion necessary for MTC. Lightly shaded spheres are xenon, darker spheres are SF_6. The infinite, periodic 3D zeolite lattice is not shown for clarity. Reprinted figure with permission from L. A. Clark, G. T. Ye, and R. Q. Snurr, *Physical Review Letters*, 84, 2893–2896, 2000. Copyright (2000) by the American physical society.

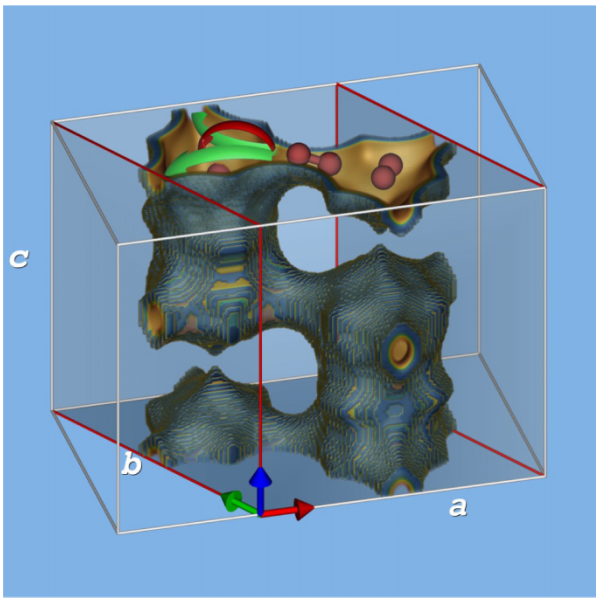

Figure 10. Molecular path control (MPC) in nanoporous materials. A periodic unit cell of erionite-type zeolite is shown. At low loading molecules diffuse twice as fast in the *c*-direction compared to the hexagonal *ab*-plane, while at higher loadings the opposite is observed due to a blockage formed by molecules at the center of the elongated cages. MPC offers the ability to direct molecules at the molecular level by simply adjusting the pressure.

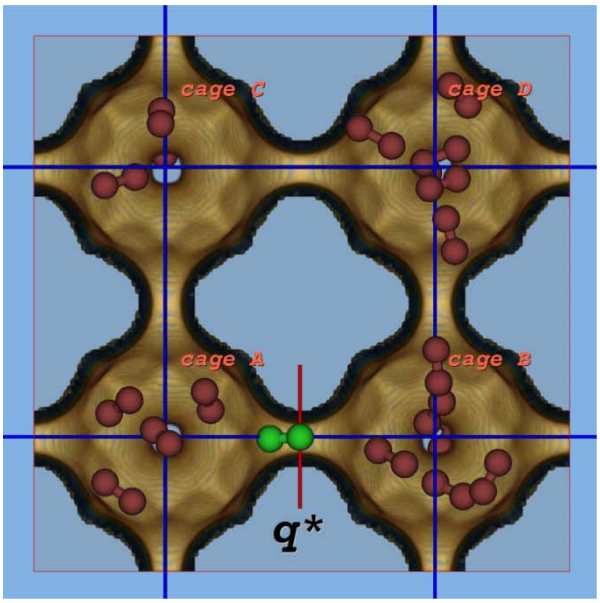

Figure 11. A typical snapshot of ethane (CH_3—CH_3) in LTA-type zeolite at an average loading of 4 molecules per cage at 750 K, constraining one tagged molecule at the dividing surface q^*. The hopping events are coarse-grained on a lattice spanned by the cage centers. Reprinted figure with permission from E. Beerdsen, B. Smit, and D. Dubbeldam, *Physical Review Letters*, 93, 248301, 2004. Copyright (2004) by the American physical society.

7. Review: transition state theory for diffusion in nanoporous materials

One of the difficulties encountered when studying diffusion in zeolites using simulation is that many processes occur outside the time scale accessible to MD, which is currently limited to diffusion rates faster than about $10^{-12}\,m^2/s$. This is a general problem, not specific to nanoporous materials, and developing new methods to overcome this time scale problem is an active area of research [153]. Systems characterized by a sequence of rare events can be described by transition state theory (TST) methods like the Bennett–Chandler approach [154,155], the chain of states method [156], the Ruiz–Montero method [157], path sampling [158], transition interface sampling [159,160], hyperdynamics [161], parallel replica dynamics [162], temperature-accelerated dynamics [163], and on-the-fly kinetic Monte Carlo [164]. In principle, all of these methods have the potential to be orders of magnitude more efficient than normal MD while still retaining full atomistic detail.

In TST approximations, one computes a rate constant for hopping between states A and B by computing the equilibrium particle flux through the dividing surface. The dividing surface should partition the system into two well-defined states, where the reaction coordinate describes the progress of the diffusion event from state A to state B. In many structures the reaction coordinate follows directly from the geometry of the confinement. For example, in figure 11 a possible reaction coordinate for ethane in LTA-type zeolite is shown: the projection of the position of one of the beads on the *x*-axis. The location of the dividing barrier is denoted by q^*. In the Bennett–Chandler approach [154,155,55] one computes the hopping rate over the barrier in two steps:

i) the relative probability $P(q^*)$ is computed to find a particle on top of the barrier at the dividing surface q^*, relative to finding it in state A,
ii) the average velocity at the top of the barrier is computed as $\sqrt{k_BT/2\pi m}$ (assuming that the particle velocities follow a Maxwell–Boltzmann distribution), and the probability κ (dynamical correction) that the system ends up in state *B* is obtained by running short MD trajectories from the dividing surface.

The transmission rate $k_{A\to B}$ from cage A to cage B is then given by

$$k_{A\to B} = \kappa \times \sqrt{\frac{k_BT}{2\pi m}} \times P(q^*) \tag{36}$$

with

$$P(q^*) = \frac{e^{-\beta F(q^*)}}{\int_{\text{cage A}} e^{-\beta F(q)} dq}, \tag{37}$$

where $\beta = 1/(k_BT)$, k_B is the Boltzmann constant, T the temperature, m the mass involved in the reaction coordinate, and $F(q)$ the Helmholtz free energy as a function of q. Calculating TST rate constants is, therefore, equivalent to calculating free energy differences. The

exact rate can be recovered by running short MD trajectories from the dividing surface to compute a dynamical correction (dc) [55]. If dynamical corrections are of order unity, the physics of diffusion can be understood by analyzing the free energy profiles.

Many groups have worked on the time scale problem for diffusion under confinement. Theodorou *et al.* [20] have summarized some of the early work using TST in zeolites, some of which dates back to the 1970's. In 1991, June *et al.* [165] modeled self-diffusion of xenon and SF_6 in silicalite at infinite dilution as a series of uncorrelated jumps between potential energy minima (sites) using dynamically-corrected TST. The rate constants for jumping between the sites were converted to diffusivities by generating continuous-time/discrete-space Monte-Carlo random walks. The computed diffusivities were reasonably close to the values computed using conventional MD. Snurr *et al.* [166] investigated the dynamical behavior of benzene in silicalite using TST. A fully atomistic model of benzene was employed. Diffusion paths connecting pairs of potential energy minima were constructed through saddle points (transition states) and the rate constants were calculated using a harmonic approximation. Given the rate constants, the self-diffusivity was computed with a kMC simulation. Forester and Smith [167] used constrained reaction coordinate dynamics (Bluemoon ensemble) to characterize the free energy profile of benzene in silicalite at 300 K along the mean reaction path for diffusion. The free energies, combined with estimates of the transmission coefficients, were used to obtain rate constants for diffusion between the main adsorption sites. Subsequent kMC simulations provided the self-diffusion coefficients. They accounted for the zeolite flexibility, so their results matched considerably better with experiments than the results of Snurr *et al.* did. Maginn *et al.* [168] presented a hierarchical approach for simulating the low-loading diffusion of *n*-alkanes up to C_{20} in silicalite using modest computational resources with concepts from Brownian motion theory and TST. Jousse and Auerbach [169] used TST to compute exact rate coefficients for benzene jumps in Na-Y zeolite. Mossel *et al.* [170,171] studied the diffusion of benzene and *p*-xylene in zeolite NaY by means of constrained reaction coordinate dynamics. MD simulations were used to determine the potential of mean force along the coordinate perpendicular to the window connecting two supercages of the zeolite. Diffusion coefficients and activation energies were determined from a hopping model that considered dynamical corrections. Ghorai *et al.* [172] estimated the rate of passage of CCl_4 through the 8-ring window in a model of zeolite A by combining a direct evaluation of the free energy profile and an adaptation of the rare events method. The system contained on average one particle per cage, and because particle–particle interactions rarely occur under this condition the free energy was evaluated from the one-particle partition function. The self-diffusion of ethane in cation-free LTA-type zeolite has been studied by Schüring *et al.* [173] using MD and TST (without dynamical correction) for various temperatures. The bare TST jump rates were found to be similar to the MD jump rates. Both results were not corrected for short-time recrossings. The number of cage-visitations counted in MD significantly over counts the actual long-term hopping rate. A particle traveling from cage A to B can for example have a sequence of A–(B–A–B–A)–B, with the (B–A–B–A) short-time movement on top of the barrier. This should be eliminated and the sequence should be counted as one jump from A to B. Dubbeldam *et al.* [121,133] applied dcTST to study abnormal diffusion of linear alkane molecules (C_1—C_{20}) in ERI-, CHA-, and LTA-type zeolites at infinite dilution. The exceptionally slow diffusion rates required the combination of rare-event TST techniques with the configurational-bias Monte Carlo (CBMC) algorithm [55,174]. The diffusivities were evaluated on a lattice spanned by the cage centers.

It is important to note that the works described in the previous paragraph have been performed at infinite dilution, even though many industrial processes occur at high loadings. A limited number of TST studies have dealt with nonzero loading. Tunca and Ford [175] used multidimensional TST to obtain the hopping rate of adsorbates from an α-cage in LTA-type zeolite as a function of loading. Various approximations were applied to make the simulations computationally feasible. In a subsequent study [176] the limitations of an empty receiving cage and the use of the Widom insertion method were avoided. Recently, Tunca and Ford presented a new hierarchical approach to the molecular modeling of diffusion and adsorption at nonzero loading in microporous materials [177]. They computed elementary hopping rates using multidimensional TST for use in a subsequent coarse-grained kMC scheme. Although adsorption was well represented, the coarse-grained self-diffusivity calculations under-predicted the diffusivity at low loading, while significantly over-predicting the diffusivities at higher loadings in comparison to conventional MD. The modeling technique was combined with a non-equilibrium molecular simulation algorithm to provide an efficient simulation of steady-state permeation across a microporous material [178]. Gupta and Snurr studied pore blockage in silicalite zeolite using free energy perturbation calculations [179]. Binary systems consisting of large co-adsorbed molecules (*n*-hexane, cyclohexane, and benzene) with smaller penetrant molecules (methane) were simulated to investigate the mechanisms of pore blockage in silicalite. Benzene and cyclohexane trap the methane molecules in the zeolite channels on the time scales of molecular dynamics simulations. Minimum energy paths for methane diffusion past the blocking molecules were determined, and free energy perturbation calculations were carried out along the paths to get the rate constants of methane hopping past coadsorbed benzene and cyclohexane molecules, which adsorb in the channel intersections.

Recently, Beerdsen *et al.* [180] extended the dcTST Bennett–Chandler approach to include diffusion of

molecules at non-zero loading. It was shown that particle–particle correlations can be taken into account by a proper definition of an effective hopping rate of a *single* particle. The self-diffusivity was computed directly by computing the hopping rate of a molecule over a typical length scale given by the smallest repeating zeolite structure, i.e. from the center of cage A to the center of cage B. A separate kMC computation is unnecessary because the relevant correlations are already captured by this computation. Implicitly one integrates over all adsorption sites in the cage, irrespective of whether these are well-defined or not. All other particles are regarded as a contribution to the external field exerted on this tagged particle. Basically, the method proceeds similar to the infinite dilution case, but the difference is that other particles are simulated "in the background." The details of how to do this properly are described in Refs. [180,181,152]. The dcTST extension to finite loadings yielded excellent agreement with conventional MD simulations, as shown in figure 12.

As seen in figure 12, diffusion of methane in the cage-type zeolite LTA initially *increases* with loading. The free energy profiles are plotted in figure 13. The positions q_A and q_B correspond to the projected centers of the cages A and B, while $q*$ denotes the eight ring window of LTA. Note that the free energy is related to the probability of being at a specific position q as:

$$\beta F(q) = -\log[P(q)] \tag{38}$$

and a high free energy means it is very unlikely to find a particle at that position, while the low free energy regions correspond to possible adsorption sites. The free energy barrier can be energetic or entropic. (For LTA-type zeolite this barrier is entropic [173].) The reason for the increase in diffusion rate with loading is mainly an increase in the free energy inside the cages as more particles are added (the barrier region is less affected). This is due to the repulsion between the particles and the loss of possible attraction as adsorption sites are being filled up. Only at high loadings do steric hindrance and enhanced collisions result in the usual

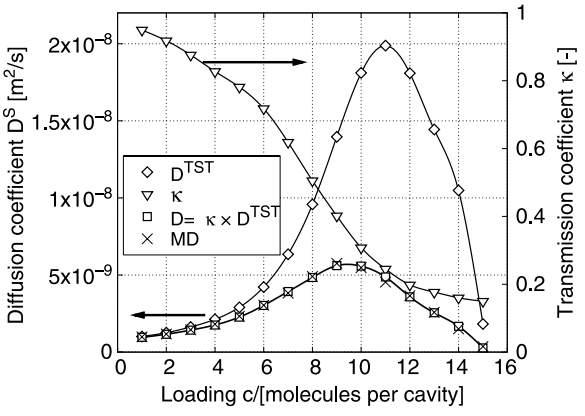

Figure 12. The TST, dcTST, and MD self-diffusivities for methane in LTA-type zeolite at 600 K as a function of loading (left axis) and the transmission coefficient κ (right axis). Reprinted figure with permission from E. Beerdsen, B. Smit, and D. Dubbeldam, *Physical Review Letters*, 93, 248301, 2004. Copyright (2004) by the American physical society.

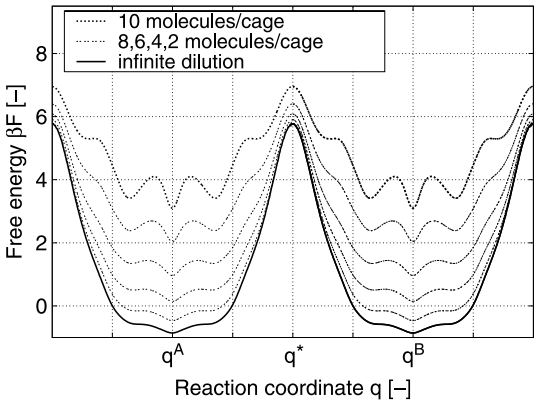

Figure 13. Free energy profiles of methane in LTA-type zeolite at 600 K for various loadings (10, 8, 6, 4, 2 molecules per cage, and infinite dilution). Reprinted figure with permission from E. Beerdsen, B. Smit, and D. Dubbeldam, *Physical Review Letters*, 93, 248301, 2004. Copyright (2004) by the American physical society.

lowering of the diffusivity with loading. This steric hindrance corresponds to the dynamical correction term, which becomes more pronounced as loading increases. The two contributions, i.e. the free energy part and the dynamical correction, are shown in figure 12.

Beerdsen *et al.* continued by using this method to make a classification scheme for methane diffusion in various zeolites by carefully analyzing the free energy profiles in relation to the zeolite structures [95,96]. Three classes could be identified as well as the reasons for their specific diffusion behavior as a function of loading.

- *Cage-type structures*

  The cage-type molecular sieves generally consist of large cages, connected by narrow windows forming large free-energy barriers. The molecule's interaction with the sieve wall is favorable. With every molecule that is added to a cage, more of this interaction is exchanged for less favorable interaction with other molecules, causing an increase in the free energy at the bottom of the well. The influence of particles at the window region is much smaller, so that as the structure is filled up, the net free-energy barrier decreases, causing an increase in both the self- and the transport-diffusion coefficients. At very high density, packing and free-volume effects cause the diffusion to decrease. LTA-, ERI-, CHA-, and SAS-type systems all conform to this scenario for the diffusion of methane. The increase in both self- and corrected-diffusion compared to the infinite dilution limit can be a surprising two orders of magnitude.
- *Unidimensional channel-type structures*

  The second class of confinement consists of channel-type molecular sieves. Upon insertion of new molecules, again the free energy in the interior of the cage rises, but this time the effect on the free energy is even larger at the barriers. As a result, the diffusivity (both D^S and D^C) is a decreasing function of loading. The details of the diffusion loading dependence depend on the exact topology of the channels. The smoother the

channel (i.e., the wider the windows with respect to the cages), the steeper the decreasing function will be. In channel-type structures, the amount of collective behavior is much higher than in cage-type structures, because the barriers are lower. The difference between D^S and D^C depends on the window size relative to the channel-size. Examples of unidimensional channel-type are MTW, AFI, and TON. It is possible to make a smooth transition from a cage-like system to a tube-like structure. LTL can be considered such a transition between the truly cage-type and the smooth channel-type molecular sieves.

- *Intersecting channel-type structures*

  The third class of confinement is the class of intersecting channel-type structures, of which MFI is the most famous example. Other examples are BEC, ISV, and BOG. Any type of structure with channels running in different directions that mutually intersect falls into this category. The barriers are formed by the horizontally aligned channels, creating entropic traps between consecutive vertical channels. The influence of loading in these systems is complex, as it involves effects such as nonsimultaneous freezing in vertical and horizontal channels, due to differences in channel diameter and length, causing varying degrees of commensurability of the particles with the structure, as a function of loading and direction. Here, like in the case of channel-type molecular sieves, the self-diffusion still sharply decreases when the loading is increased, but the corrected diffusivity initially only slightly decreases with density, until packing effects sharply decrease the corrected diffusivity as well.

Note that for all scenarios, both D^S and D^C (sharply) decrease near the maximum loading, due to packing effects that eventually reduce the diffusion to the level of solid diffusion, irrespective of the topology of the confinement, in violation of the common assumption that the corrected diffusivity is constant as a function of loading. This decrease of diffusion can be delayed to higher loading by free-energy effects: adsorbing molecules that lower the free-energy barrier have a favorable effect on the diffusion. The loading at which the final decrease sets in is determined by the size of the cage and the topology of the confinement.

Beerdsen *et al.* stress that the ordering of molecular sieve structures in classes depends strictly on the combination of adsorbate and adsorbent. The method was developed using methane in zeolites as examples, but it should be readily adaptable to other adsorbates and other materials such as MOFs.

8. Experiment vs. simulation

Comparison of diffusion coefficients from simulation with experimental results is complicated by existing disagreements among experimental results from different measurement techniques. The discrepancies between experimental methods have provided the motivation for development of a number of new methods for measuring diffusion in microporous materials [2]. There is often disagreement among results from microscopic (PFG NMR, QENS), mesoscopic (micro-FT IR), and macroscopic (membrane permeation, uptake methods, zero length column, frequency response) techniques, although results from within a given class (microscopic, mesoscopic, macroscopic) often agree. A recent review by Kärger addresses the main problems associated with the determination and interpretation of molecular diffusion in zeolites [182]. He points out that the diffusivities in zeolites may depend significantly on the relevant length and time scales of observation, as well as on the experimental conditions under which the measurements are carried out. It must also be kept in mind that some techniques measure self-diffusivities and others measure transport diffusivities. In order to resolve discrepancies among results from different techniques, collaborative research projects have been initiated to make comparative diffusion measurements for selected systems under similar conditions by different experimental techniques [183–185].

In general, the microscopic methods often agree very well with molecular simulation results. For example, figure 14(b) shows the results of Chong *et al.* [186] for ethane in silicalite. Using parameters that reproduce the adsorption isotherms (figure 14(a)), they were able to predict the self-diffusivity (not shown), the corrected diffusivity, and the transport diffusivity as functions of loading in excellent agreement with results from QENS. QENS is often in better agreement with molecular simulation than PFG NMR, which probes longer length scales. This (and other evidence in recent years) suggests that the results of different measurement methods that differ in magnitude are not necessarily in "disagreement", but they probe different aspects of diffusion on different time and length scales. Molecular simulations use "perfect" crystals without defects, whereas real zeolite samples will always contain some imperfections. These disordered defects will be probed differently by different measurement techniques. Recent simulations of Beerdsen and Smit suggest that simulation and experimental data compared at the *same* loading correspond with each other much better than expected [187]. Leroy and Jobic studied the diffusion of *n*-octane in silicalite using QENS and simulations [188]. A larger diffusivity was found when compared with previous experiments performed in Na-ZSM-5, by a factor of four, allowing a further reduction of the gap between experiment and simulation. Diffusion behavior in the siliceous form of zeolites and their aluminosilicate analogues can potentially be very different, even when few cations are present.

Another promising future development is a paper by García-Pérez *et al.* [189]. The aluminum distribution on the crystal level, as well as the distribution on a single unit cell level, remains a subject of debate. García-Pérez *et al.* presented an alternative theoretical approach in which they identified those experimentally accessible properties that are crucially dependent on the details of the aluminum distribution and associated cation distribution. Once these

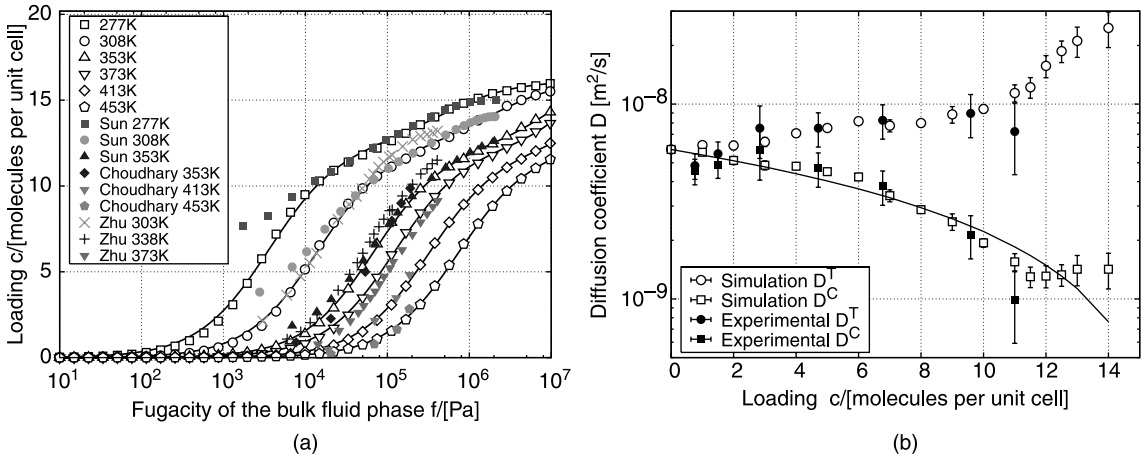

Figure 14. Comparison of simulation and experimental results. (a) Adsorption isotherms for ethane in silicalite. Simulation model parameters and references for experimental adsorption data are given in Refs. [36,37]. (b) Corrected and transport diffusion coefficients for ethane in silicalite as functions of loading from the work of Chong *et al.* [186]. Note that the same model and parameters were used to predict all thermodynamic and transport properties shown. Reprinted figure (a) with permission from D. Dubbeldam, S. Calero, T. J. H. Vlugt, R. Krishna, T. L. M. Maesen, E. Beerdsen and B. Smit, *Physical Review Letters*, 93, 088302, 2004. Copyright (2004) by the American physical society. Figure (b) reprinted from chemical physics letters, 408, S. Chong, H. Jobic, M. Plazanet, D. S. Sholl, Concentration dependence of transport diffusion of ethane in Silicalite: a comparison between neutron scattering experiments and atomically-detailed simulations, 157–161, Copyright (2005), with permission from Elsevier.

properties had been identified, they computed the most likely position of aluminum in zeolites by matching simulation results with available experimental data. The approach is guided by the results obtained from advanced molecular simulations in two groups of structures. The first group—with adsorption properties insensitive to aluminum distribution- was previously used to unambiguously parameterize their simulation method. Aluminum positions on the second group of structures influence their adsorptive and diffusive properties and they show that this might be exploited to reverse-engineer the average aluminum distribution using molecular simulations. Of course this crucially depends on the quality of the force field. Recently, three force fields were developed for sodium, calcium and protons in aluminosilicalites that gave not only qualitatively good results in agreement with experiments, but also quantitatively [38–40]. These force fields were additionally validated in Refs. [190,191]. Again, when simulation and experiment were performed under equivalent conditions, in this case the same aluminum distribution (and therefore, the same average cation distribution), the results were in very good agreement.

For mixtures, methane and CF_4 in silicalite has become a useful reference system because experimental measurements exist for single-component and binary adsorption isotherms [192] and for single-component and binary self-diffusivities [64]. MD and GCMC predictions using the same potential model are in good agreement with these results.

9. Conclusions and future directions

Simulation of diffusion of adsorbed molecules in crystalline nanoporous materials has advanced considerably in recent years. These advances have been made possible by a combination of algorithmic developments and growing computer power. Early studies used EMD simulations mainly to calculate the self-diffusivity for single-component diffusion. Studies of binary self-diffusion followed, and recently researchers have used equilibrium MD and non-equilibrium MD to calculate the Fickian and Maxwell–Stefan diffusivities and the Onsager coefficients for binary systems. These MD results have played an important role in the development of theoretical models for predicting multicomponent diffusion in zeolites from single-component data. The ability to examine the molecular-level details of sorbate motion has also shed light on difficult problems such as the window effect, incommensurate diffusion, and molecular traffic control. An on-going challenge in MD and GCMC studies in zeolites is the need for accurate potential models, particularly for heteroatoms in the zeolites and for adsorbate molecules with more interesting chemical functional groups.

Much progress has been made in developing methods to overcome the inherent time-scale limitations of MD simulation. However, significant challenges remain in this area. For example, work has focused only on calculating the self-diffusivities, but methods are also needed to calculate the corrected diffusivities for slowly-diffusing systems. Methods to simulate combined reaction and diffusion over relevant time scales would also be useful.

Diffusion studies in MOFs have been reported in only a small number of papers to date. Given the potential applications of these materials, this is a promising area for future work. Studies to date have noted the similarity to diffusion in zeolites. However, it is likely that MOF structures are considerably more flexible than zeolites. Experimental and simulation studies of MOF flexibility and its affect on adsorption and diffusion should be quite

interesting. This is clearly a challenging problem for both experiments and simulation.

Acknowledgements

This work has been supported by the National Science Foundation (CTS-0302428 and CTS-0507013). We thank R. Krishna for valuable suggestions and comments on the manuscript and D. S. Sholl for providing the data of figure 14.

References

[1] D.M. Ruthven. *Principles of Adsorption and Adsorption Processes*, John Wiley & Sons, New York, NY (1984).
[2] J. Kärger, D.M. Ruthven. *Diffusion in Zeolites and Other Microporous Solids*, John Wiley & Sons Inc., New York, NY (1992).
[3] H. van Bekkum, E.M. Flanigen, P.A. Jacobs,, J.C. Jansen (Eds.). *Introduction to Zeolite Science and Practice*, 2nd ed., Elsevier, Amsterdam (2001).
[4] N.Y. Chen, T.F. Degnan Jr., C.M. Smith. *Molecular Transport and Reaction in Zeolites*, VCH Publishers, New York, NY (1994).
[5] M.E. Davis. Ordered porous materials for emerging applications. *Nature*, **417**, 813 (2002).
[6] A. Stein. Advances in microporous and mesoporous solids – highlights of recent progress. *Adv. Mater.*, **15**, 763 (2003).
[7] T.L. Barton, L.M. Bull, W.G. Klemperer, D.A. Loy, B. McEnaney, M. Misono, P.A. Monson, G. Pez, G.W. Scherer, J.C. Vartuli, O.M. Yaghi. Tailored porous materials. *Chem. Mater.*, **11**, 2633 (1999).
[8] P.J. Stang, B. Olenyuk. Self-assembly, symmetry, and molecular architecture: Coordination as the motif in the rational design of supramolecular metallacyclic polygons and polyhedra. *Acc. Chem. Res.*, **30**, 502 (1997).
[9] M. Fujita. Metal-directed self-assembly of two- and three-dimensional synthetic receptors. *Chem. Soc. Rev.*, **27**, 417 (1998).
[10] M. Eddaoudi, D. Moler, H. Li, B. Chen, T.M. Reineke, M. O'Keeffe, O.M. Yaghi. Modular chemistry: Secondary building units as a basis for the design of highly porous and robust metal-organic carboxylate frameworks. *Acc. Chem. Res.*, **34**, 319 (2001).
[11] P.H. Dinolfo, J.T. Hupp. Supramolecular coordination chemistry and functional microporous molecular materials. *Chem. Mater.*, **13**, 3113 (2001).
[12] S. James. Metal-organic frameworks. *Chem. Soc. Rev.*, **32**, 276 (2003).
[13] C. Janiak. Engineering coordination polymers toward applications. *Dalton Trans.*, **14**, 2781 (2003).
[14] O.M. Yaghi, M. O'Keeffe, N.W. Ockwig, H.K. Chae, M. Eddaoudi, J. Kim. Reticular synthesis and the design of new materials. *Nature*, **423**, 705 (2003).
[15] J.L.C. Rowsell, O.M. Yaghi. Metal-organic frameworks: A new class of porous materials. *Micropor. Mesopor. Mater.*, **73**, 3 (2004).
[16] S. Kitagawa, R. Kitaura, S. Noro. Reticular synthesis and the design of new materials. *Nature*, **423**, 705 (2003).
[17] H.S. Fogler. *Elements of Chemical Reaction Engineering*, 2nd ed., PTR Prentice Hall, Englewood Cliffs, New Jersey, NJ (1992).
[18] R.Q. Snurr, J.T. Hupp, S.T. Nguyen. Prospects for nanoporous metal-organic materials in advanced separations processes. *AIChE J.*, **50**, 1090 (2004).
[19] U. Mueller, M. Schubert, F. Teich, H. Puetter, K. Schierle-Arndt, J. Pastre. Metal-organic frameworks – prospective industrial applications. *J. Mater. Chem.*, **16**, 626 (2006).
[20] D.N. Theodorou, R.Q. Snurr, A.T. Bell. *Comprehensive Supramolecular Chemistry*, G. Alberti, T. Bein (Eds.), Vol. 7, Chapter 18, pp. 507–548, Pergamon Oxford, Oxford (1996).
[21] P. Demontis, G.B. Suffritti. Structure and dynamics of zeolites investigated by molecular dynamics. *Chem. Rev.*, **97**, 2845 (1997).
[22] S.M. Auerbach. Theory and simulation of jump dynamics, diffusion and phase equilibrium in nanopores. *Int. Rev. Phys. Chem.*, **19**(2), 155 (2000).
[23] F.J. Keil, R. Krishna, M.O. Coppens. Modeling of diffusion in zeolites. *Rev. Chem. Eng.*, **16**, 71 (2000).
[24] S.M. Auerbach, F. Jousse, D.P. Vercauteren. Dynamics of sorbed molecules in zeolites. *Computer Modelling of Microporous and Mesoporous Materials*, C.R.A. Catlow, R.A. van Santen, B. Smit (Eds.), Academic Press, London (2002).
[25] D.S. Sholl. Understanding macroscopic diffusion of adsorbed molecules in crystalline nanoporous materials via atomistic simulations. *Acc. Chem. Res.*, **39**, 403 (2006).
[26] A.G. Bezus, A.V. Kiselev, A.A. Lopatkin, P.Q.J. Du. Molecular statistical calculation of thermodynamic adsorption characteristics of zeolites using atom-atom approximation .1. Adsorption of methane by zeolite NaX. *J. Chem. Soc. Faraday Trans. II*, **74**, 367 (1978).
[27] A.H. Fuchs, A.K. Cheetham. Adsorption of guest molecules in zeolitic materials: Computational aspects. *J. Phys. Chem. B*, **105**, 7375 (2001).
[28] M.G. Martin, J.I. Siepmann. Transferable potentials for phase equilibria. 1. United-atom description of *n*-alkanes. *J. Phys. Chem. B*, **102**, 2569 (1998).
[29] M.G. Martin, J.I. Siepmann. Novel configurational-bias Monte Carlo method for branched molecules. Transferable potentials for phase equilibria. 2. United-atom description of branched alkanes. *J. Phys. Chem. B.*, **103**, 4508 (1999).
[30] P. Demontis, G.B. Suffritti, S. Quartieri, E.S. Fois, A. Gamba. Molecular dynamics on zeolites 3. Dehydrated zeolite-A. *J. Phys. Chem.*, **92**, 867871 (1988).
[31] J.B. Nicholas, A.J. Hopfinger, F.R. Trouw, L.E. Iton. Molecular modeling of zeolite structure .2. Structure and dynamics of silica sodalite and silicate force-field. *J. Am. Chem. Soc.*, **113**, 4792 (1991).
[32] T.J.H. Vlugt, M. Schenk. Influence of framework flexibility on the adsorption properties of hydrocarbons in the zeolite silicalite. *J. Phys. Chem. B*, **106**, 12757 (2002).
[33] J.A. Greathouse, M.D. Allendorf. The interaction of water with MOF-5 simulated by molecular dynamics. *J. Am. Chem. Soc.*, **128**, 10678 (2006).
[34] F. Leroy, B. Rousseau, A.H. Fuchs.Self-diffusion of *n*-alkanes in silicalite using molecular dynamics simulation: A comparison between rigid and flexible frameworks. *Phys. Chem. Chem. Phys.*, **406**, 775 (2004).
[35] L.J. Broadbelt, R.Q. Snurr. Applications of molecular modeling in heterogeneous catalysis research. *Appl. Catal. A*, **200**, 23 (2000).
[36] D. Dubbeldam, S. Calero, T.J.H. Vlugt, R. Krishna, T.L.M. Maesen, E. Beerdsen, B. Smit. Force field parametrization through fitting on infection points in isotherms. *Phys. Rev. Lett.*, **93**, 088302 (2004).
[37] D. Dubbeldam, S. Calero, T.J.H. Vlugt, R. Krishna, T.L.M. Maesen, B. Smit. United atom force field for alkanes in nanoporous materials. *J. Phys. Chem. B*, **108**, 12301 (2004).
[38] S. Calero, D. Dubbeldam, R. Krishna, B. Smit, T.J.H. Vlugt, J.F.M. Denayer, J.A. Martens, T.L.M. Maesen. Understanding the role of sodium during adsorption: A force field for alkanes in sodium-exchanged faujasites. *J. Am. Chem. Soc.*, **126**, 11377 (2004).
[39] S. Calero, M.D. Lobato, E. García-Pérez, J.A. Mejias, S. Lago, T.J.H. Vlugt, T.L.M. Maesen, B. Smit, D. Dubbeldam. A coarse-graining approach for the proton complex in protonated aluminosilicates. *J. Phys. Chem. B*, **110**, 5838 (2006).
[40] E. García-Pérez, D. Dubbeldam, T.L.M. Maesen, S. Calero. Influence of cation Na/Ca ratio on adsorption in LTA 5A: A systematic molecular simulation study of alkane chain length. *J. Phys. Chem. B*, **110**(47), (2006).
[41] S. Chempath, R.Q. Snurr, J.J. Low. Molecular modeling of binary liquid-phase adsorption of aromatics in silicalite. *AIChE J.*, **50**, 463 (2004).
[42] S. Chempath, J.F.M. Denayer, K.M.A. De Meyer, G.V. Baron, R.Q. Snurr. Adsorption of liquid-phase alkane mixtures in silicalite: Simulations and experiment. *Langmuir*, **20**, 150 (2004).
[43] T. Ala-Nissila, R. Ferrando, S.C. Ying. Collective and single particle diffusion on surfaces. *Adv. Phys.*, **51**, 949 (2002).
[44] H. Jobic, J. Karger, M. Bee. Simultaneous measurement of self- and transport diffusivities in zeolites. *Phys. Rev. Lett.*, **82**(21), 4260 (1999).
[45] J.A. Wesselingh, R. Krishna. *Mass Transfer in Multicomponent Mixtures*, Delft University Press, Delft (2000).
[46] R. Krishna, R. Baur. Modelling issues in zeolite based separation processes. *Sep. Purif. Technol.*, **33**, 213 (2003).

[47] R. Krishna, J.M. van Baten. Describing binary mixture diffusion in carbon nanotubes with the Maxwell-Stefan equations. An investigation using molecular dynamics simulations. *Ind. Eng. Chem. Res.*, **45**, 2084 (2006).

[48] R. Krishna, J.M. van Baten. Diffusion of alkane mixtures in zeolites: Validating the Maxwell-Stefan formulation using MD simulations. *J. Phys. Chem. B*, **109**, 6386 (2005).

[49] J.M. van Baten, R. Krishna. Entropy effects in adsorption and diffusion of alkane isomers in mordenite: An investigation using CBMC and MD simulations. *Micropor. Mesopor. Mater.*, **84**, 179 (2005).

[50] D. Paschek, R. Krishna. Inter-relation between self-and jump-diffusivities in zeolites. *Chem. Phys. Lett.*, **333**, 278 (2001).

[51] R. Krishna, D. Paschek. Self-diffusivies in multicomponent mixtures in zeolites. *Phys. Chem. Chem. Phys.*, **4**, 1891 (2002).

[52] A.I. Skoulidas, D.S. Sholl. Direct tests of the Darken approximation for molecular diffusion in zeolites using equilibrium molecular dynamics. *J. Phys. Chem. B*, **105**, 3151 (2001).

[53] M.P. Allen, D.J. Tildesley. *Computer Simulation of Liquids*, Clarendon Press, Oxford (1987).

[54] D.C. Rapaport. *The Art of Molecular Dynamics Simulation*, 2nd ed., Cambridge University Press, Cambridge (2004).

[55] D. Frenkel, B. Smit. *Understanding Molecular Simulation*, 2nd ed., Academic Press, London, UK (2002).

[56] D.A. Reed, G. Ehrlich. Surface diffusivity and the time correlation of concentration fluctuations. *Surf. Sci.*, **105**, 603 (1981).

[57] K. Kremer, G.S. Grest. Dynamics of entangled linear polymer melts – a molecular-dynamics simulation. *J. Chem. Phys.*, **92**, 5057 (1990).

[58] S. Jakobtorweihen, C.P. Lowe, F.J. Keil, B. Smit. A novel algorithm to model the infuence of host lattice flexibility in molecular dynamics simulations: Loading dependence of self-diffusion in carbon nanotubes. *J. Chem. Phys.*, **124**, 154706 (2006).

[59] S. Jakobtorweihen, M.G. Verbeek, C.P. Lowe, F.J. Keil, B. Smit. Understanding the loading dependence of self-diffusion in carbon nanotubes. *Phys. Rev. Lett.*, **95**, 044501 (2005).

[60] A.I. Skoulidas, D.M. Ackerman, J.K. Johnson, D.S. Sholl. Rapid transport of gases in carbon nanotubes. *Phys. Rev. Lett.*, **89**, 185901 (2002).

[61] H.B. Chen, D.S. Sholl. Rapid diffusion of CH_4/H_2 mixtures in single-walk carbon nanotubes. *J. Am. Chem. Soc.*, **126**, 7778 (2004).

[62] H.B. Chen, J.K. Johnson, D.S. Sholl. Transport diffusion of gases is rapid in flexible carbon nanotubes. *J. Phys. Chem. B*, **110**, 1971 (2006).

[63] G. Arora, N.J. Wagner. Adsorption and diffusion of molecular nitrogen in single wall carbon nanotubes. *Langmuir*, **20**, 6268 (2004).

[64] R.Q. Snurr, J. Kärger. Molecular simulation and NMR measurements of binary diffusion in zeolites. *J. Phys. Chem. B*, **101**, 6469 (1997).

[65] S. Jost, N.-K. Bär, S. Fritzsche, R. Haberlandt, J. Kärger. Diffusion of a mixture of methane and xenon in silicalite: A molecular dynamics study and pulsed field gradient nuclear magnetic resonance experiments. *J. Phys. Chem. B*, **102**, 6375 (1998).

[66] L.N. Gergidis, D.N. Theodorou. Molecular dynamics simulation of *n*-butane/methane mixtures in silicalite. *J. Phys. Chem. B*, **103**, 3380 (1999).

[67] E.J. Maginn, A.T. Bell, D.N. Theodorou. Transport diffusivity of methane in silicalite from equilibrium and nonequilibrium simulations. *J. Phys. Chem.*, **97**, 4173 (1993).

[68] B.J. Berne, R. Pecora. *Dynamic Light Scattering*, p. 86, Wiley, New York, NY (1976).

[69] S. Fritzsche, R. Haberlandt, J. Kärger. An MD study on the correlation between transport diffusion and self-diffusion in zeolites. *Z. Phys. Chemie*, **189**, 211 (1995).

[70] G. Heffelfinger, F.V. Swol. Diffusion in Lennard–Jones fluids using dual control volume grand canonical molecular dynamics simulation (DCV GCMD). *J. Chem. Phys.*, **100**, 7548 (1994).

[71] J.M.D. MacElroy. Nonequilibrium molecular dynamics simulation of diffusion and flow in thin microporous membranes. *J. Chem. Phys.*, **101**, 5274 (1994).

[72] M.G. Ahunbay, J.R. Elliott, O. Talu. The diffusion process of methane through a silicalite single crystal membrane. *J. Phys. Chem. B*, **106**, 5163 (2002).

[73] G. Arya, H.C. Chang, E.J. Maginn. A critical comparison of equilibrium, non-equilibrium and boundary-driven molecular dynamics techniques for studying transport in microporous material. *J. Chem. Phys.*, **115**, 8112 (2001).

[74] S. Chempath, R. Krishna, R.Q. Snurr. Nonequilibrium molecular dynamics simulation of diffusion in binary mixtures containing short *n*-alkanes in faujasite. *J. Phys. Chem. B*, **108**, 13481 (2004).

[75] H.L. Tepper, W.J. Briels. Comments on the use of the Einstein equation for transport diffusion: Application to argon in $AlPO_4$-5. *J. Chem. Phys.*, **116**, 9464 (2002).

[76] J.P. Hoogenboom, H.L. Tepper, N.F.A. van der Vegt, W.J. Briels. Transport diffusion of argon in $AlPO_4$-5 from equilibrium molecular dynamics simulations. *J. Chem. Phys.*, **113**, 6875 (2000).

[77] D.S. Sholl. Predicting single-component permeance through macroscopic zeolite membranes from atomistic simulations. *Ind. Eng. Chem. Res.*, **39**, 3737 (2000).

[78] J.-P. Boon, Y. Sip. *Molecular Hydrodynamics*, McGraw Hill, New York, NY reprinted by Dover, 1991. (1980).

[79] G.K. Papadopoulus, H. Jobìc, D.N. Theodorou. Transport diffusivity of N_2 and CO_2 in silicalite: coherent quasielastic neutron scattering measurements and molecular dynamics simulations. *J. Phys. Chem. B*, **108**, 12748 (2004).

[80] R. Krishna, J.M. van Baten. MD simulations of diffusivities in methanol – *n*-hexane mixtures near the liquid-liquid phase splitting region. *Chem. Eng. Technol.*, **29**, 516 (2006).

[81] R. Krishna, J.M. van Baten, D. Dubbeldam. On the infection in the concentration dependence of the Maxwell–Stefan diffusivity of CF_4 in MFI zeolite. *J. Phys. Chem. B*, **108**, 14820 (2004).

[82] M.J. Sanborn, R.Q. Snurr. Diffusion of binary mixtures of CF_4 and *n*-alkanes in faujasite. *Sep. Purif. Technol.*, **20**, 1 (2000).

[83] M.J. Sanborn, R.Q. Snurr. Predicting membrane flux of CH_4 and CF_4 mixtures in faujasite from molecular simulations. *AIChE J.*, **47**, 2032 (2001).

[84] A.I. Skoulidas, D.S. Sholl, R. Krishna. Correlation effects in diffusion of CH_4/CF_4 mixtures in MFI zeolite. A study linking MD simulations with the Maxwell–Stefan formulation. *Langmuir*, **19**, 7977 (2003).

[85] R. Krishna, J.M. van Baten. Linking the loading dependence of the Maxwell–Stefan diffusivity of linear alkanes in zeolites with the thermodynamic correction factor. *Chem. Phys. Lett.*, **420**, 545 (2006).

[86] A.L. Myers, J.M. Prausnitz. Thermodynamics of mixed-gas adsorption. *AIChE J.*, **11**, 121 (1965).

[87] R. Krishna, D. Paschek, R. Baur. Modeling the occupancy dependence of diffusivities in zeolites. *Micropor. Mesopor. Mater.*, **76**, 233 (2004).

[88] R. Krishna, J.M. van Baten. Kinetic Monte Carlo simulations of the loading dependence of diffusion in zeolites. *Chem. Eng. Technol.*, **28**, 160 (2005).

[89] R. Krishna, J.M. van Baten. Influence of isotherm inflection on the diffusivities of C_5-C_8 linear alkanes in MFI zeolite. *Chem. Phys. Lett.*, **407**, 159 (2005).

[90] R. Krishna, J.M. van Baten. The Darken relation for multi-component diffusion in liquid mixtures of linear alkanes. An investigation using molecular dynamics (MD) simulations. *Ind. Eng. Chem. Res.*, **44**, 6939 (2005).

[91] H. Jobic, N. Laloué, C. Laroche, J. van Baten, R. Krishna. Influence of isotherm inflection on the loading dependence of the diffusivities of *n*-hexane and *n*-heptane in MFI zeolite. Quasi-elastic neutron scattering experiments supplemented by molecular simulations. *J. Phys. Chem. B*, **110**, 2195 (2006).

[92] D.S. Sholl. Testing predictions of macroscopic binary diffusion coeffcients using lattice models with site heterogeneity. *Langmuir*, **22**, 3707 (2006).

[93] A. Skoulidas, D.S. Sholl. Transport diffusivities of CH_4, CF_4, He, Ne, Ar, Xe, and SF_6 in silicalite from atomistic simulations. *J. Phys. Chem. B*, **106**, 5058 (2002).

[94] A. Skoulidas, D.S. Sholl. Molecular dynamics simulations of self-diffusivities, corrected diffusivities, and transport diffusivities of light gases in four silica zeolites to assess influences of pore shape and connectivity. *J. Phys. Chem. A*, **107**, 10132 (2003).

[95] E. Beerdsen, D. Dubbeldam, B. Smit. Understanding diffusion in nanoporous materials. *Phys. Rev. Lett.*, **96**, 044501 (2006).

[96] E. Beerdsen, D. Dubbeldam, B. Smit. Loading dependence of the diffusion coefficient of methane in nanoporous materials. *J. Phys. Chem. B*, 110(45), 22754 (2006).

[97] E. Beerdsen, D. Dubbeldam, B. Smit. Molecular understanding of diffusion in confinement. *Phys. Rev. Lett.*, **95**, 164505 (2005).

[98] L. Sarkisov, T. Düren, R.Q. Snurr. Molecular modelling of adsorption in novel nanoporous metal-organic materials. *Mol. Phys.*, **102**, 211 (2004).

[99] A.I. Skoulidas. Molecular dynamics simulations of gas diffusion in metal-organic frameworks: Argon in Cu-BTC. *J. Am. Chem. Soc.*, **126**, 1356 (2004).

[100] A.I. Skoulidas, D.S. Sholl. Self-diffusion and transport diffusion of light gases in metal-organic framework materials assessed using molecular dynamics simulation. *J. Phys. Chem. B*, **109**, 15760 (2005).

[101] Q.Y. Yang, C.L. Zhong. Molecular simulation of adsorption and diffusion of hydrogen in metal-organic frameworks. *J. Phys. Chem. B*, **109**, 11862 (2005).

[102] F. Stallmach, S. Gröger, V. Künzel, J. Kärger, O.M. Yaghi, M. Hesse, U. Müller. NMR studies on the diffusion of hydrocarbons on the metal-organic framework material MOF-5. *Angew. Chem. Int. Ed.*, **45**, 2123 (2006).

[103] O.F. Sankey, P.A. Fedders. Generalized atomic hopping problem – particle correlation-functions. *Phys. Rev. B*, **15**, 3586 (1977).

[104] P.A. Fedders, O.F. Sankey. Generalized atomic hopping problem – occupancy correlation-functions. *Phys. Rev. B*, **15**, 3580 (1977).

[105] J. Kärger. Straightforward derivation of the long-time limit of the mean-square displacement in one-dimensional diffusion. *Phys. Rev. A*, **45**, 4173 (1992).

[106] A.L. Hodgkin, R.D. Kenes. The potassium permeability of a giant nerve fibre. *J. Physiol. (London)*, **128**, 61 (1955).

[107] S.D. Druger, A. Nitzan, M.A. Ratner. Dynamic bond percolation theory – a micropscopic model for diffusion in dynamically disorderd-systems.1. Definition and one-dimensional case. *J. Chem. Phys.*, **79**, 3133 (1983).

[108] V. Kukla, J. Kornatowski, D. Demuth, I. Girnus, H. Pfeifer, L.V.C. Rees, S. Schunk, K.K. Unger, J. Kärger. NMR studies of single-file diffusion in unidimensional channel zeolites. *Science*, **272**, 702 (1996).

[109] K. Hahn, J. Kärger, V. Kukla. Single-file diffusion observation. *Phys. Rev. Lett.*, **76**, 2762 (1996).

[110] V. Gupta, S.S. Nivarthi, A.V. McCormick, H.T. Davis. NMR studies of single-file diffusion in unidimensional channel zeolites. *Chem. Phys. Lett.*, **247**, 596 (1995).

[111] C. Lutz, M. Kollmann, C. Bechinger. Single-file diffusion of colloids in one-dimensional channels. *Phys. Rev. Lett.*, **93**, 026001 (2004).

[112] S.S. Nivarthi, A.V. McCormick, H.T. Davis. Diffusion anisotropy in molecular sieves – a Fourier-transform PFG NMR-study of methane in $AlPO_4$-5. *Chem. Phys. Lett.*, **299**, 297 (1994).

[113] H. Jobic, K. Hahn, J. Kärger, M. Bee, A. Tuel, M. Noack, I. Girnus, G.J. Kearley. Unidirectional and single-file diffusion of molecules in one-dimensional channel systems. A quasi-elastic neutron scattering study. *J. Phys. Chem. B*, **101**, 5834 (1997).

[114] V. Gupta, S.S. Nivarthi, D. Keffer, A.V. McCormick, H.T. Davis. Evidence of single-file diffusion in zeolites. *Science*, **274**, 164 (1996).

[115] K.F. Czaplewski, T.L. Reitz, Y.J. Kim, R.Q. Snurr. One-dimensional zeolites as hydrocarbon traps. *Micropor. Mesopor. Mater.*, **56**, 55 (2002).

[116] N.Y. Chen, S.J. Lucki, E.B. Mower. Cage effect on product distribution from cracking over crystalline alumnosilicate zeolites. *J. Catal.*, **13**, 329 (1969).

[117] N. Chen, W.E. Garwood, F.G. Dwyer. *Shape Selective Catalysis in Industrial Applications*, 2nd Edition, Revised and Expanded. Chemical Industries, New York, NY (1996).

[118] J. Weitkamp, S. Ernst, L. Puppe. *Catalysis and Zeolites*, J. Weitkamp, L. Puppe (Eds.), pp. 326–376, Springer, Berlin (1999).

[119] J.A. Martens, P.A. Jacobs. *Zeolite Microporous Solids: Synthesis, Structure, and Reactivity*, E.G. Derouane, F. Lemos, C. Naccache, F. Ramão-Ribeiro (Eds.), Vol. 36, pp. 511–529, Kluwer, Amsterdam (1992).

[120] R.L. Gorring. Diffusion of normal parafins in zeolite T occurrence of a window effect. *J. Catal.*, **31**, 13 (1973).

[121] D. Dubbeldam, S. Calero, T.L.M. Maesen, B. Smit. Incommensurate diffusion in confined systems. *Phys. Rev. Lett.*, **90**, 245901 (2003).

[122] D. Dubbeldam, S. Calero, T.L.M. Maesen, B. Smit. Understanding the window effect in zeolite catalysis. *Angew. Chem. Int. Ed.*, **42**, 3624 (2003).

[123] Y.I. Frenkel, T. Kontorowa. Über die theorie der plastischen verformung. *Phys. Z. Sowietunion*, **13**, 1 (1938).

[124] T. Kontorowa, Y.I. Frenkel. On the theory of plastic deformation and twinning i, ii. *Zh. Eksp. Teor. Fiz.*, **8**(89), 1340 (1938a).

[125] O.M. Braun, Y. Kivshar. Nonlinear dynamics of the Frenkel-Kontorova model. *Phys. Rep.*, **306**, 1 (1998).

[126] P.M. Chaikin, T.C. Lubensky. *Principles of Condensed Matter Physics*, Cambridge University Press, Cambridge (1995).

[127] E. Ruckenstein, P.S. Lee. Resonant diffusion. *Phys. Lett. A*, **56**, 423 (1976).

[128] E.G. Derouane, J.M. Andre, A.A. Lucas. Surface curvature effects in physisorption and catalysis by microporous solids and molecular sieves. *J. Catal.*, **110**, 58 (1988).

[129] J.M. Nitsche, J. Wei. Window effects in zeolite diffusion and Brownian motion over potential barriers. *AIChE J.*, **37**, 661 (1991).

[130] C.L.C. Jr, M. Eić, D.M. Ruthven, M.L. Occelli. Diffusion of *n*-parafins in offretiteerionite type zeolites. *Zeolites*, **15**, 293 (1995).

[131] F.D. Magalhães, R.L. Laurence, W.C. Conner. Transport of *n*-parafins in zeolite T. *AIChE J.*, **42–86**, 68 (1996).

[132] D.M. Ruthven. The window effect in zeolitic diffusion. *Micropor. Mesopor. Mater.*, 262 (2006).

[133] D. Dubbeldam, B. Smit. Computer simulation of incommensurate diffusion in zeolites: Understanding window effects. *J. Phys. Chem. B*, **107**, 12138 (2003).

[134] K. Yoo, R. Tsekov, P.G. Smirniotus. Experimental proof for resonant diffusion of normal alkanes in LTL and ZSM-12 zeolites. *J. Phys. Chem. B*, **7**, 13593 (2003).

[135] H. Jobic, A. Méthivier, G. Ehlers, B. Farago, W. Haeussler. Accelerated diffusion of long-chain alkanes between nanosized cavities. *Angew. Chem. Int. Ed.*, **43**, 364 (2004).

[136] R. Tsekov, E. Evstatieva. Resonant diffusion on modulated surfaces. *Adv. Coll. Interf. Surf.*, **114**, 159 (2005).

[137] R. Tsekov, P.G. Smirniotis. Resonant diffusion of normal alkanes in zeolites: Effect of the zeolite structure and alkane molecule vibrations. *J. Phys. Chem. B*, **102**, 9385 (1998).

[138] R.C. Runnebaum, E.J. Maginn. Resonant diffusion of normal alkanes in zeolites: Effect of the zeolite structure and alkane molecule vibrations. *J. Phys. Chem. B*, **101**, 6394 (1997).

[139] O. Talu, M.S. Sun, D.B. Shah. Diffusivities of *n*-alkanes in silicalite by steady-state single-crystal membrane technique. *AIChE J.*, **44**, 681 (1998).

[140] H. Jobic, J. Molec. Diffusion of linear and branched alkanes in ZSM-5. a quasi-elastic neutron scattering study. *Catal. A Chem.*, **158**, 135 (2000).

[141] S. Yashonath, P. Santikary. Diffusion of sorbates in zeolite Y and zeolite A – novel dependence on sorbate size and strength of sorbate-zeolite interaction. *J. Phys. Chem.*, **98**, 6368 (1994).

[142] C. Rajappa, S. Yashonath. Levitation effect and its relationship with the underlying potential energy landscape. *J. Chem. Phys.*, **110**, 5960 (1999).

[143] P.K. Ghorai, S. Yashonath. Classification of the third regime in the size dependence of self diffusivity in levitation effect. *Chem. Phys. Lett.*, **402**, 222 (2005).

[144] P.K. Ghorai, S. Yashonath, P. Demontis, G.B. Suffritti. Diffusion anomaly as a function of molecular length of linear molecules: Levitation effect. *J. Am. Chem. Soc.*, **125**, 7116 (2003).

[145] C.R. Kamala, K.G. Ayappa, S. Yashonath. Large distinct diffusivity in binary mixtures confined to zeolite NaY. *J. Phys. Chem. B*, **109**, 22092 (2005).

[146] E.G. Derouane, Z. Gabelica. A novel effect of shape selectivity – molecular traffic control in zeolite ZSM-5. *J. Catal.*, **65**, 486 (1980).

[147] L.A. Clark, G.T. Ye, R.Q. Snurr. Molecular traffic control in a nonoscale system. *Phys. Rev. Lett.*, **84**, 2893 (2000).

[148] P. Bräuer, A. Brzank, J. Kärger. Adsorption and reaction in single-file networks. *J. Phys. Chem. B*, **107**, 1821 (2003).

[149] N. Neugebauer, P. Bräuer, J. Kärger. Reactivity enhancement by molecular traffic control. *J. Catal.*, **194**, 1 (2000).

[150] P. Bräuer, N. Neugebauer, J. Kärger. A simple jump model for describing the molecular traffic control effect. *Coll. Surf.*, **187**, 459 (2001).

[151] D. Dubbeldam, E. Beerdsen, S. Calero, B. Smit. Molecular path control in zeolite membranes. *Proc. Natl. Acad. Sci. USA*, **102**, 12317 (2005).

[152] D. Dubbeldam, E. Beerdsen, S. Calero, B. Smit. Dynamically corrected transition state theory calculations of self-diffusion in

anisotropic nanoporous materials. *J. Phys. Chem. B*, **110**, 3164 (2006).
[153] A.F. Voter, F. Montalenti, T.C. Germann. Extended the time scale in atomistic simulation of materials. *Annu. Rev. Mater. Res.*, **32**, 321 (2002).
[154] C.H. Bennett. *Diffusion in Solids: Recent Developments*, A. Nowick, J. Burton (Eds.), pp. 73–113, Academic Press, New York, NY (1975).
[155] D. Chandler. Statistical mechanics of isomerization dynamics in liquids and the transition state approximation. *J. Chem. Phys.*, **68**, 2959 (1978).
[156] E.M. Sevick, A.T. Bell, D.N. Theodorou. A chain of states method for investigating infrequent event processes occuring in multistate, multidimensional systems. *J. Chem. Phys.*, **98**, 3196 (1993).
[157] M.J. Ruiz-Montero, D. Frenkel, J.J. Brey. Efficient schemes to compute diffusive barrier crossing rates. *Mol. Phys.*, **90**, 925 (1996).
[158] P.G. Bolhuis, C. Dellago, D. Chandler. Sampling ensembles of deterministic transition pathways. *Faraday Disc.*, **110**, 421 (1998).
[159] T.S. van Erp, D. Moroni, P.G. Bolhuis. A novel path sampling method for the calculation of rate constants. *J. Chem. Phys.*, **118**, 7762 (2003).
[160] D. Moroni, P.G. Bolhuis, T.S. van Erp. Rate constants for diffusive processes by partial path sampling. *J. Chem. Phys.*, **120**, 4055 (2004).
[161] A.F. Voter. Hyperdynamics: Accelerated molecular dynamics of infrequent events. *Phys. Rev. Lett.*, **78**, 3908 (1997).
[162] A.F. Voter. Parallel replica method for dynamics of infrequent events. *Phys. Rev. B*, **57**, 13985 (1998).
[163] M.R. Sorensen, A.F. Voter. Temperature-accelerated dynamics for simulation of infrequent events. *J. Chem. Phys.*, **112**, 9599 (2000).
[164] G. Henkelman, H. Jónsson. Long time scale kinetic Monte Carlo simulations without lattice approximation and predefined event table. *J. Chem. Phys.*, **115**, 9657 (2001).
[165] R.L. June, A.T. Bell, D.N. Theodorou. Transition-state studies of xenon and SF_6 diffusion in silicate. *J. Phys. Chem.*, **95**, 8866 (1991).
[166] R.Q. Snurr, A.T. Bell, D.N. Theodorou. Investigation of the dynamics of benzene in silicate using transition-state theory. *J. Phys. Chem.*, **98**, 11948 (1994).
[167] T.R. Forester, W. Smith. Bluemoon simulations of benzene in silicalite-1 – prediction of free energies and diffusion coefficients. *J. Chem. Soc. Faraday Trans.*, **93**, 3249 (1997).
[168] E.J. Maginn, A.T. Bell, D.N. Theodorou. Dynamics of long *n*-alkanes in silicalite: a hierarchical simulation approach. *J. Phys. Chem.*, **100**, 7155 (1996).
[169] F. Jousse, S.M. Auerbach. Activated diffusion of benzene in NaY zeolite: Rate constants from transition state theory with dynamical corrections. *J. Chem. Phys.*, **107**, 9629 (1997).
[170] T. Mosell, G. Schrimpf, J. Brickmann. Diffusion of aromatic molecules in zeolite NaY .1. Constrained reaction coordinate dynamics. *J. Phys. Chem. B*, **101**, 9476 (1997).
[171] T. Mosell, G. Schrimpf, J. Brickmann. Diffusion of aromatic molecules in zeolite NaY .2. Dynamical corrections. *J. Phys. Chem. B*, **101**, 9485 (1997).
[172] P.K. Ghorai, S. Yashonath, R.M. Lynden-Bell. Estimation of slow diffusion rates in confined systems: CCl_4 in zeolite NaA. *Mol. Phys.*, **100**, 641 (2002).
[173] A. Schüring, S.M. Auerbach, S. Fritzsche, R. Haberlandt. On entropic barriers for diffusion in zeolites: A molecular dynamics study. *J. Chem. Phys.*, **116**, 10890 (2002).
[174] B. Smit, J.I. Siepmann. Computer simulations of the energetics and siting of *n*-alkanes in zeolites. *J. Phys. Chem.*, **98**, 8442 (1994).
[175] C. Tunca, D.M. Ford. A transition-state theory approach to adsorbate dynamics at arbitrary loadings. *J. Chem. Phys.*, **111**, 2751 (1999).
[176] C. Tunca, D.M. Ford. Modeling cage-to-cage dynamics of adsorbates at arbitrary loadings with dynamically corrected transition-state theory. *J. Phys. Chem. B*, **106**, 10982 (2002).
[177] C. Tunca, D.M. Ford. A hierarchical approach to the molecular modeling of diffusion and adsorption at nonzero loading in microporous materials. *Chem. Eng. Sci.*, **58**, 3373 (2003).
[178] C. Tunca, D.M. Ford. Coarse-grained nonequilibrium approach to the molecular modeling of permeation through microporous membranes. *J. Chem. Phys.*, **120**, 10763 (2004).
[179] A. Gupta, R.Q. Snurr. A study of pore blockage in silicalite zeolite using free energy perturbation calculations. *J. Phys. Chem. B*, **109**, 1822 (2005).
[180] E. Beerdsen, B. Smit, D. Dubbeldam. Molecular simulation of loading dependent slow diffusion in confined systems. *Phys. Rev. Lett.*, **93**, 248301 (2004).
[181] D. Dubbeldam, E. Beerdsen, T.J.H. Vlugt, B. Smit. Molecular simulation of loading-dependent diffusion in nanopoxous materials using extended dynamically corrected transition state theory. *J. Chem. Phys.*, **122**, 224712 (2005).
[182] J. Kärger. Measurement of diffusion in zeolites – a never ending challenge? *Adsorption*, **9**, 29 (2003).
[183] J. Kärger, D. Ruthven. Diffusion in zeolites. *J. Chem. Soc. Faraday Trans. 1*, **77**, 1485 (1981).
[184] J. Kärger, D. Ruthven. Self-diffusion and diffusive transport in zeolite crystals. *Stud. Surf. Sci. Catal.*, **105**, 1843 (1997).
[185] H. Jobic, J. Kärger, C. Krausse, S. Brandani, A. Gunadi, A. Methivier, G. Ehlers, B. Farago, W. Haeussler, D.M. Ruthven. Diffusivities of *n*-alkanes in 5A zeolite measured by neutron spin echo, pulsed-field gradient NMR, and zero length column techniques. *Adsorption*, **11**, 403 (2005).
[186] S. Chong, H. Jobic, M. Plazanet, D.S. Sholl. Concentration dependence of transport diffusion of ethane in silicalite: A comparison between neutron scattering experiments and atomically-detailed simulations. *Chem. Phys. Lett.*, **408**, 157 (2005).
[187] E. Beerdsen, B. Smit. Diffusion in confinement: Agreement between experiments better than expected. *J. Phys. Chem. B*, **110**, 14529 (2006).
[188] F. Leroy, H. Jobic. Influence of extra-framework cations on the diffusion of alkanes in silicalite: Comparison between quasi-elastic neutron scattering and molecular simulations. *Chem. Phys. Lett.*, **406**, 375 (2005).
[189] E. García-Pérez, D. Dubbeldam, B. Liu, B. Smit, S. Calero. A computational method to characterize framework aluminium in aluminosillicates. *Angew. Chem. Int. Ed.*, 46(7–2), 276 (2006).
[190] B. Liu, B. Smit. Molecular simulation of adsorption of alkanes in sodium MOR-type zeolites using a new force. *Phys. Chem. Chem. Phys.*, **8**, 1852 (2006).
[191] B. Liu, B. Smit, S. Calero. Evaluation of a new force field for describing the adsorption behavior of alkanes in various pure silica zeolites. *J. Phys. Chem. B*, 110(41), 20166 (2006).
[192] M. Heuchel, R.Q. Snurr, E. Buss. Adsorption of CH_4-CF_4 mixtures in silicatlie: Simulation, experiment, and theory. *Langmuir*, **13**, 6795 (1997).